DME/TACAN Multipath Impact on GNSS L5/E5a Airborne Receivers Part I: C/N0 Degradation Model

NICOLAS GAULT
AXEL GARCIA-PENA
ALEXANDRE CHABORY
CHRISTOPHE MACABIAU
LOÏC SHI-GARRIER
École Nationale de l'Aviation Civile, Toulouse, France

This article is the first part of a two-part manuscript addressing the DME/TACAN multipath impact on the future airborne GNSS L5/E5a receivers. Part I updates the multipath-free (MP-free) statistical C/N_0 degradation model due to DME/TACAN in presence of a temporal blanker, which relies on the definition of the above blanker pulse width ($\mathrm{pw}^{\mathrm{eq}}$) and the below blanker equivalent pulse width ($\mathrm{PW}^{\mathrm{eq}}$). In presence of multipath (MP), $\mathrm{pw}^{\mathrm{eq}}$ and $\mathrm{PW}^{\mathrm{eq}}$ are updated and customized for two different set of assumptions: the statistical and the fixed environment assumptions. Under the statistical assumption, the additional phase offset generated by the environment θ_{e} is assumed to follow an uniform law. Under this assumption, $\mathrm{pw}^{\mathrm{eq}}$ and $\mathrm{PW}^{\mathrm{eq}}$ are updated and closed-form formulas are found for $\mathrm{pw}^{\mathrm{eq}}$ and $\mathrm{PW}^{\mathrm{eq}}$. Under the fixed environment assumption, θ_{e} is assumed to be constant over a short observation time T_0. Under this modelling, $\mathrm{pw}^{\mathrm{eq}}$ and $\mathrm{PW}^{\mathrm{eq}}$ formulas are updated but analytical formulas may not be found if received pulses don't keep their Gaussian shapes due to collisions. Therefore, zones where the closed forms formulas of $\mathrm{pw}^{\mathrm{eq}}$ and $\mathrm{PW}^{\mathrm{eq}}$ from the statistical model may be used under the fixed environment assumption are defined and illustrated in a simple configuration.

I. INTRODUCTION

The nominal processing of Global Navigation Satellite System (GNSS) received signals can be affected by noise as well as received additive signals such as multipath (MP) and Radio Frequency Interference (RFI) [1]. GNSS L5/E5a interference environment is predominantly dominated by pulsed interferences such as DME/TACAN and JTIDS/MIDS [1], [2]. In the context of civil aviation, the RFI impact on a GNSS receiver is internationally standardized by the International Civil Aviation Organization (ICAO), in the United States by the Radio Technical Commission for Aeronautics (RTCA) and in Europe by the European Organization for Civil Aviation Equipment (EUROCAE). In the standards of these standardization bodies, the RFI impact is usually modelled as the C/N_0 degradation, which is determined as the difference between the nominal C/N_0 and the effective C/N_0, $C/N_{0,eff}$. The effective C/N_0 is defined as the C/N_0 observed at the receiver antenna port where the noise power generated at the correlator output by the equivalent noise with PSD $N_{0,eff}$ is equal to the power generated by a noise with PSD equal to N_0 plus the power generated by the analyzed RFI signals. The definition of effective C/N_0 assumes that the receiver Radio Frequency Front End (RFFE) elements, i.e. the Low Noise Amplifier (LNA), Mixer, Radio Frequency (RF) and Intermediate Frequency (IF) filters, Automatic Gain Control/Analog to Digital Converter (ADC/AGC) [1],[2],[3] as well as the correlator are ideal.

To mitigate the impact of the pulsed RFI observed in the L5/E5a band, a temporal blanker in the RFFE block is assumed to be implemented by the civil aviation standards in Dual-Frequency Multi-Constellation (DFMC) GNSS receivers [1],[4]. The role of the blanker is to set to zeros the received signal samples having its instantaneous power envelope higher than a certain threshold (interference detection). Considering the blanker, RTCA DO-292 [1] proposes a statistical model of the C/N_0 degradation as a function of the percentage of samples set to zero by the blanker, denoted as blanker duty cycle, (bdc), and the below-blanker interfering-signal-to-thermal-noise ratio, R_{I} [1]-[4].

The values of bdc and R_{I} depend on the RFI scenario (number of emitting beacons, interference received power at the aircraft antenna port, etc.) and a worst-case scenario was found at Harrisburg P.A, at high altitude (FL400), where the C/N_0 degradation was determined equal to 7.34 dB, after correcting the identified numerical error in [1]. Along the elaboration of the update of [1], several improvements, namely on the blanker implementation [5], the DME/TACAN interference environment [6] and assumptions on pulses collisions and post-blanker pulsed interference Power Spectrum Density (PSD) [7], were already proposed in the past.

Another improvement of [1] would be the inclusion of DME/TACAN multipath (MP) impact in the proposed C/N_0 degradation model. Indeed, the DME/TACAN beacons/aircraft RFI scene is such that the DME/TACAN beacons situated on the ground transmit a signal near the L5 frequency (1176.45 MHz) to the aircraft situated at an altitude range from a few hundred of meters to several kilometers and a slant range from the beacons of a few tens of kilometers from the beacons. In this scene, many elements (buildings, electric pylons, trees etc.) situated in the Radio Line Of Sight (RLOS) of the emitting DME/TACAN beacons are generating MP and must be considered, even if the scattered power may be very small. The elements generating MP are designated as scatterers in this study. For a more complete characterization of the DME/TCAN beacons/aircraft propagation channel, the reader is referred to Part II of this work [8].

DME/TACAN pulses received from MP are denoted as echoed pulses or echoes in this work. MP can be a threat for

the future airborne DFMC receiver since echoed pulses impact the receiver in the same manner as the direct pulse: echoes could trigger the blanking threshold and thus increase bdc or simply increase R_I. For these reasons, a DME/TACAN MP analysis must be conducted in order to assess the impact of MP in the overall C/N_0 degradation. More specifically, the R_I and bdc analytical models must be updated to correctly consider echoes. To the best knowledge of the authors, no MP effect on the C/N_0 degradation computation are considered in the literature.

Therefore, the general objective of this paper is to update the R_I and bdc analytical models proposed in [1] to accurately consider echoes in the C/N_0 degradation computation. In particular, two models are proposed: the statistical and the fixed environment models.

The statistical model assumes that the additional phase offset generated by any physical effect produced by the DME/TACAN beacon/aircraft environment as the weather or the random scatterers properties (constructions, closed shutters etc.) is assumed to follow an uniform law on $[0,2\pi[$. This model allows to find a statistical average of the C/N_0 degradation for a single point in a given aircraft trajectory assuming all environmental conditions are unknown.

The fixed environment model assumes that the phase offset produced by the physical effects of the canal can be assumed to be constant over $[t, t+T_0]$ where T_0 does not exceed 1 s. This model allows to find a statistical average of the C/N_0 degradation for a small part of an aircraft trajectory.

The statistical model presented in this work is later used in Part II of this two-parts manuscript to determine the additional C/N_0 degradation due to DME/TACAN only generated by echoed pulses at two low-altitude operational hot-spots: JALTO (USA) FAF and TIXAK (Europe) FAF, which are two single points of the approach of the Philadelphia and Frankfurt airports [8]. Note that the proposed statistical model was initially presented in [9] by the same authors but never mathematically demonstrated.

The article is organized as follows. Section II provides an overview of the DME/TACAN system and signal description and the current C/N_0 degradation model as described in [1]. Section III introduces the statistical C/N_0 degradation model considering MP. Section IV presents the fixed environment C/N_0 degradation model considering MP. Section V concludes the analysis.

II. CURRENT STATISTICAL DME/TACAN C/N_0 DEGRADATION MODEL

In this section, the DME/TACAN system and signal description, as well as the current C/N_0 degradation and its application to DME/TACAN pulsed interference are presented.

A. DME/TACAN System and Signal Description

In this section, the system operation as well as a close description of the received DME/TACAN signal at the aircraft antenna's output are introduced. DME, and its military equivalent, TACAN, are two systems used by aircrafts to determine their distance to a position-known ground beacon. The airborne interrogator sends interrogations to the beacons. Once the interrogation is detected, the beacon transponder replies to the interrogation. The slant range (distance between the two systems) is then determined by measuring the time elapsed between each pulse transmitted by the interrogator and the reception of its corresponding reply pulse from the transponder. This delay corresponds to twice the distance between the aircraft and the beacon, as well as a fixed processing time inside the ground station. Full systems operation is described in [10].

The only threat for future DFMC airborne receivers are the reply pulses emitted by the beacon transponder operating in mode X as they emit their signals between 962 and 1213 MHz, which overlaps the GNSS L5/E5a band, equal to [1166.45; 1186.45] MHz [1]. The beacon transponder replies are thus the RFI investigated in this work. Without MP, a single beacon emitted reply $s_{\mathrm{bb}}(t)$ at baseband is a composite pulse composed of two Gaussian pulses such that

$$\begin{aligned} s_{\mathrm{bb}}(t) &= g(t) + g(t-\Delta t) \\ g(t) &= e^{-\frac{\alpha}{2}t^2}, \end{aligned} \tag{1}$$

where $\alpha = 4.5 \cdot 10^{11}\ \mathrm{s}^{-2}$ is a constant of pulse and $\Delta t = 12\ \mu s$ is the inter pulse time separation for mode X. Fig. 1 (green curve) provides an example of a baseband emitted pair. The signal s_{bb} is then modulated by a cosine before its broadcasting to the aircraft. Fig. 1 (blue curve) provides an example of a modulated emitted pair in presence of noise.

Multiple aircrafts are simultaneously communicating with different beacons and therefore multiple replies may be received by a single aircraft. Therefore, the received signal $r(t)$ at an aircraft's receiving antenna port without considering multipath is modelled as, during an observation period $[0, T_0]$,

$$\begin{aligned} r(t) &= \sum_{m=1}^{M} \sum_{\kappa}^{\mathrm{K}_m} A_m s_{\mathrm{bb}}\left(t - t_m^{\kappa} - \tau_m(t)\right) \cdot \\ &\qquad \cos\left(2\pi\left(f_m + f_{D,m}\right)t + \theta_m^{\kappa}\right), \\ A_m &= \sqrt{2\mathrm{PEP}_m} \end{aligned} \tag{2}$$

The index m is used to identify the different broadcasting beacons, where M is the number of DME/TACAN emitting beacons.

The index κ is used to identify the emitted pulse pair, where K_m is the number of pulse pairs sent by beacon m during $[0, T_0]$ assumed to be known. When the time of observation T_0 is long enough, K_m can be assumed to be equal to $\mathrm{PRF} \cdot T_0$, where PRF is the average pair repetition frequency: 2700 Hz for DME and 3600 Hz for TACAN.

The scalars A_m and PEP_m are the amplitude and peak envelope power of the received pairs from beacon m assumed to be constant inside $[0, T_0]$, respectively.

The random variable t_m^κ is the emitted time of pair κ from beacon m and is modelled to follow an uniform distribution over $[0, T_0]$ ($t_m^\kappa \sim U[0, T_0]$), as the emission rate of emitted pairs is assumed to follow a Poisson process [1] and K_m is assumed to be known.

The scalar $\tau_m(t)$ is the propagation time delay associated which evolves with time. Using first-order Taylor's expansion, $\tau_m(t)$ is approximated as

$$\tau_m(t) = \tau_m(0) + t \left.\frac{d\tau_m(t)}{dt}\right|_{t=0}. \quad (3)$$

The frequencies f_m and $f_{D,m}$ are the carrier and Doppler frequencies of beacon m, respectively. The expression of $f_{D,m}$ is given by, from (3),

$$f_{D,m} = -2\pi f_m \left.\frac{d\tau_m(t)}{dt}\right|_{t=0}. \quad (4)$$

The random variable θ_m^κ is the carrier phase offset of emitted pair κ of beacon m, modelled as

$$\theta_m^\kappa = \theta_{0,m}^\kappa + \theta_{\mathrm{D},m} + \theta_{\mathrm{e},m} \bmod 2\pi, \quad (5)$$

where the initial phase $\theta_{0,m}^\kappa$ is the phase generated at each pair k of beacon m generation. Assuming that the transponder is switched on and off each time a pulse pair is emitted, $\theta_{0,m}^\kappa$ can be modelled as an uniform variable on $[0,2\pi)$ and is independent for $m \neq m'$ and $\kappa \neq \kappa'$. The phase $\theta_{\mathrm{D},m}$ is the additional carrier phase due to the initial propagation time delay $\tau_m(0)$, i.e., from (3),

$$\theta_{\mathrm{D},m} = -2\pi f_m \tau_m(0). \quad (6)$$

Finally, the additional phase offset $\theta_{\mathrm{e},m}$ is the offset introduced by the physical effects generated by the propagation channel environment (weather, etc.). Physical effects are assumed not to change between pulse pair emissions (and thus $\theta_{\mathrm{e},m}$ does not to depend on κ) given the relatively low time interval between pulse emission (as high as 1.4 ms as specified in [10]). Its mathematical modelling depends on the targeted application/analysis; two different assumptions are considered in this work; the statistic assumption in Section III.A and the fixed environment assumption in Section IV.A, respectively.

B. Current RTCA DO-292 Statistical C/N_0 Degradation Model

The MP-free C/N_0 degradation model proposed in [1] aims at providing a statistical average of the C/N_0 degradation generated by DME/TACAN for a single aircraft position. In that case, propagation time delay $\tau_m(t)$ is a constant for all t and is thus denoted as τ_m. Additionally, the time of observation T_0 representing the time where the aircraft is in the same position is assumed to be very short.

Furthermore, at the aircraft position, the additional phase offset due to the propagation channel physical effects $\theta_{\mathrm{e},m}$ is assumed by [1] to be unknown and thus $\theta_{\mathrm{e,m}}$ is modelled as a uniform variable over $[0,2\pi)$ independent for $m \neq m'$ (since the DME/TACAN beacons are not located at the same location). In other words, the C/N_0 degradation is derived by averaging all the possible additional phase outcomes in $[0,2\pi[$.

To summarize, the modelling of the three random variables t_m^κ, $\theta_{0,m}^\kappa$ and $\theta_{\mathrm{e},m}$ of the received signal $r(t)$ assumed by [1] is

$$\begin{aligned} t_m^\kappa &\sim U[0,T_0],\ t_m^\kappa \perp \theta_{m'}^{\kappa'},\ \forall\, m,m',\kappa,\kappa', \\ \theta_{0,m}^\kappa &\sim U[0,2\pi),\ \theta_{0,m}^\kappa \perp \theta_{0,m'}^{\kappa'},\ \forall \binom{m}{\kappa} \neq \binom{m'}{\kappa'}, \\ \theta_{\mathrm{e},m} &\sim U[0,2\pi),\ \theta_{\mathrm{e},m} \perp \theta_{\mathrm{e},m'},\ \forall m \neq m', \\ \theta_{\mathrm{e},m} &\perp \theta_{0,m'}^\kappa,\ \forall\, m,m',\kappa. \end{aligned} \quad (7)$$

where $\binom{m}{\kappa} \neq \binom{m'}{\kappa'}$ means that at least $m \neq m'$ or $n \neq n'$ and $\perp$ means independent. Under this modeling, the general $\mathrm{C/N_0}$ degradation model and the MP-free bdc and $\mathrm{R_I}$ mathematical models are provided below.

General C/N_0 degradation model: The counter-measure selected by civil aviation standards to mitigate the pulsed RFI impact such as DME/TACAN or JTIDS/MIDS signals is the introduction of a temporal blanker as the last stage of the RFFE block of the future DMFC receivers (note that the final implementation depends on the receiver manufacturer since the temporal blanker exact structure is not standardized). The temporal blanker is a device which blanks (put to 0) the I/Q time samples of the incoming signal (mix of signals) from the ADC/AGC which have an instantaneous power envelope over a given threshold, $\mathrm{T_H}$. The instantaneous power envelope, $P_m(t)$, of a single Gaussian pulse generated by beacon m is defined as

$$P_m(t) = \mathrm{PEP}_m |g(t)|^2 = \mathrm{PEP}_m e^{-\alpha t^2}. \quad (8)$$

Note that for an optimal functioning of the GNSS receiver, AGC and temporal blanker must be coupled. Fig. 1 illustrates the instantaneous blanker application as defined in [1].

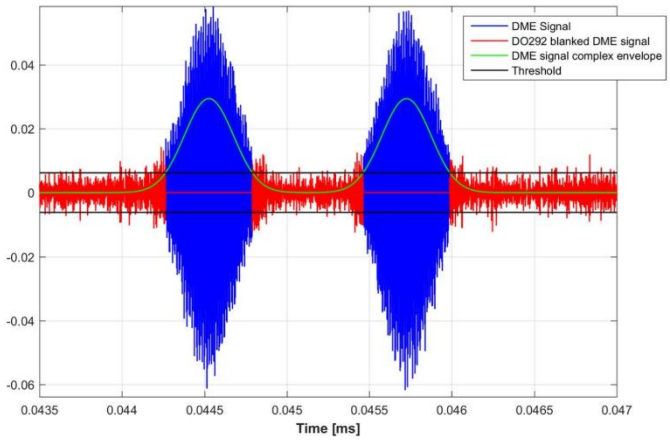

Fig. 1. Illustration of the RTCA DO-292 instantaneous blanker behavior over the DME signal

Finally, digitized and blanked signals are fed to the correlator. The impact of the RFI signals and blanking process are measured at the output of the correlator. The chosen figure of merit is the effective C/N_0 denoted as $C/N_{0,\text{eff}}$. $N_{0,\text{eff}}$ represents the effective noise power spectrum density that a receiver will observe at the antenna port which generates the same power at the correlator output as the power generated by the nominal noise with PSD equal to N_0 plus the power generated by the analyzed interferences, when assuming that all RFFE elements and the correlator are ideal. The difference between the $C/N_{0,\text{eff}}$ when only the useful signal is present, $C/N_{0,\text{eff}}^{\text{nom}}$, and the $C/N_{0,\text{eff}}$ when the useful signal and the RFI are present, $C/N_{0,\text{eff}}^{\text{RFI}}$, is called the C/N_0 degradation denoted as $\left(\frac{C}{N_0}\right)_{\text{deg}}$.

The mathematical model proposed by in [1] for $N_{0,\text{eff}}$ in presence of RFI is

$$N_{0,\text{eff}}^{\text{RFI}} = \frac{N_O}{1-\text{bdc}} \cdot \left(1 + \frac{I_{0,\text{WB}}}{N_0} + R_\text{I}\right) \tag{9}$$

where N_0 is the thermal noise power spectrum density, bdc is the blanker duty cycle which represents the percentage of time the RFI signals trigger the blanker, $I_{0,WB}$ is the equivalent white noise contribution of wideband (non-pulsed) RFI and R_I is the below-threshold interfering-signal-to-thermal-noise ratio which represents the contribution of the unblanked part of the RFI signals. Further discussion about this model can be found in [7].

In the framework of this paper, DME/TACAN are assumed to be the only RFI present at the correlator outputs and therefore $I_{0,\text{WB}} = 0$. Finally, since bdc and R_I are equal to zero when no RFI are present ($N_{0,\text{eff}}^{\text{nom}} = N_0$), the C/N_0 degradation in dB is expressed as

$$\left(\frac{C}{N_0}\right)_{deg} = 10\log_{10}\left(\frac{N_{0,\text{eff}}^{\text{RFI}}}{N_{0,\text{eff}}^{\text{nom}}}\right) = 10\log_{10}\left(\frac{1-\text{bdc}}{1+R_\text{I}}\right). \tag{10}$$

The definition of bdc and R_I assuming only DME/TACAN and without MP are presented below.

Multipath-free DME/TACAN bdc mathematical model: In this section, bdc, pw_m^{eq}, $I_{\text{bdc},m}$, l_m and r_m are defined and illustrated in Fig. 2 for an above-threshold composite pulse (two Gaussian pulses in the MP-free case). Note that the definition of pw_m^{eq} is particularly important since its model will be updated with the introduction of MP.

The RTCA DO-292 MP-free DME/TACAN bdc mathematical model is based on a Queueing Theory approach [11] and is mathematically expressed as [1],

$$\text{bdc} = 1 - e^{-\sum_{m=1}^{M} \text{pw}_m^{\text{eq}} \text{PRF}_m}, \tag{11}$$

where pw_m^{eq} is the above blanker width generated by any received composite pulse κ_0 in $[\![1, \text{K}_m]\!]$ of source m.

An important property of pw_m^{eq} is that it is invariant by translation, i.e., the delay of the first received pulse $t_m^{\kappa_0} + \tau_m$ of the composite pulse does not matter. It is thus chosen at 0 to simplify the derivation as represented in Fig. 2. In that case pw_m^{eq} is expressed as

$$\text{pw}_m^{\text{eq}} = \mu\left(I_{\text{bdc},m}\right), \tag{12}$$

where $I_{\text{bdc},m}$ is the blanked interval generated by the received composite pulse κ_0 and μ is the unidimensional Lebesgue measure, i.e., $\mu([a,b]) = b - a$. Since the composite pulse is composed of two disjoint Gaussian pulses in the MP-free case (1), $I_{\text{bdc},m}$ is decomposed in two blanked intervals as

$$I_{\text{bdc},m} = I_{\text{bdc},m}^0 \amalg I_{\text{bdc},m}^1, \tag{13}$$

where $I_{\text{bdc},m}^0$ and $I_{\text{bdc},m}^1$ are the blanked intervals generated by the first and the second pair of the composite pulse, respectively. For example, $I_{\text{bdc},m}^0$ is mathematically expressed as

$$I_{\text{bdc},m}^0 = \begin{cases} \{\emptyset\} \text{ if } \text{PEP}_m \leq \text{T}_\text{H} \\ [\text{l}_m^0, \text{r}_m^0] \text{ otherwise,} \end{cases} \tag{14}$$

where T_H is the blanking threshold and l_m^0 and r_m^0 are the instant of time when the pulse starts and stops to be blanked, respectively. Assume that $\text{PEP}_m > \text{T}_\text{H}$, the mathematical expression of l_m^0 and r_m^0 is obtained by equalizing the instantaneous peak power envelope (8) of the first pulse, $P_m(t)$ to T_H, i.e.,

$$\begin{aligned} P_m(t) = \text{T}_\text{H} \Leftrightarrow \begin{cases} \text{l}_m^0 = -w_m \\ \text{r}_m^0 = w_m, \end{cases} \\ w_m = \sqrt{\ln\left(\frac{\text{PEP}_m}{\text{T}_\text{H}}\right)/\alpha} \end{aligned} \tag{15}$$

and thus $I^0_{\mathrm{bdc},m} = [-w_m, w_m]$. The blanked interval $I^1_{\mathrm{bdc},m}$ is obtained applying exactly the same methodology but to a pulse delayed by Δt and thus $I^1_{\mathrm{bdc},m} = [\Delta t - w_m, \Delta t + w_m]$. Finally, in the MP-free case, $\mathrm{pw}_m^{\mathrm{eq}}$ is given by from (12), using the σ-additivity of the Lebesgue measure,

$$\mathrm{pw}_m^{\mathrm{eq}} \quad = \quad \mu\left(I^0_{\mathrm{bdc},m}\right) + \mu\left(I^1_{\mathrm{bdc},m}\right) = 4w_m \qquad (16)$$

which concludes the derivation of bdc in the MP-free case.

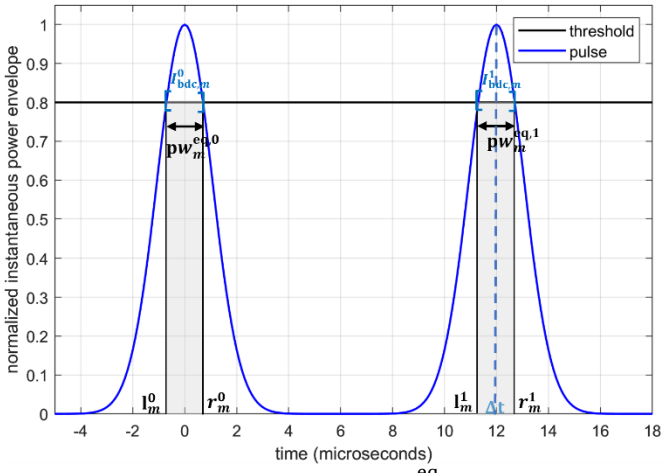

Fig. 2. Graphical illustration of $\mathrm{pw}_m^{\mathrm{eq}}, I_{\mathrm{bdc},m}$, l_m and r_m parameters for an above-threshold composite pulse in the MP-free case.

Multipath-free DME/TACAN R_{I} mathematical model: Under the statistical assumption (7), the MP-free mathematical model of R_{I} as proposed by [12] is given by

$$R_{\mathrm{I}} = \sum_{m=1}^{M} \frac{P_{\mathrm{r},m}}{N_0 \beta_0} \cdot SSC(\Delta f_m), \qquad (17)$$

where β_0 is the thermal noise power degradation due to RFFE filter and correlator, $SSC(\Delta f_i)$ is the Spectral Separation Coefficient of the pulsed interfering source m as expressed in [7] and $P_{\mathrm{r},m}$ is the post-blanker average power of the received RFI signal. This last term is of particular importance since it can be decomposed to define a new quantity $\mathrm{PW}_m^{\mathrm{eq,pulse}}$ as

$$P_{\mathrm{r},m} \quad = \quad \mathrm{PEP}_m \mathrm{PW}_m^{\mathrm{eq}} \mathrm{PRF}_m, \qquad (18)$$

where $\mathrm{PW}_m^{\mathrm{eq}}$ is the width of a rectangular pulse with amplitude PEP_m and same energy as any post-blanker received composite pulse κ_0 in $[\![1, \mathrm{K}_m]\!]$ of source m. As for $\mathrm{pw}_m^{\mathrm{eq}}$, $\mathrm{PW}_m^{\mathrm{eq}}$ is translation invariant, and therefore $t_m^{\kappa_0} + \tau_m$ is chosen at 0 to simplify the derivation.

Under the statistical assumption, $\mathrm{PW}_m^{\mathrm{eq}}$ is modelled by [1] as

$$\mathrm{PW}_m^{\mathrm{eq}} \quad = \quad \mathrm{PW}_m^{\mathrm{eq},0} + \mathrm{PW}_m^{\mathrm{eq},1}, \qquad (19)$$

where $\mathrm{PW}_m^{\mathrm{eq},0}$ and $\mathrm{PW}_m^{\mathrm{eq},1}$ are the equivalent pulse widths of the first and the second pulse of the received composite pulse, respectively.

With this definition, $\mathrm{PW}_m^{\mathrm{eq},0}$ and $\mathrm{PW}_m^{\mathrm{eq},1}$ are obtained by equalizing the energy of the first and the second pulse of the composite pulse to a rectangular pulse whose amplitude is PEP_m, i.e., from (8),

$$\begin{aligned} \mathrm{PW}_m^{\mathrm{eq},0} &= \frac{1}{\mathrm{PEP}_m} \int_{\mathbb{R}} P_m(t) b_m(t) dt \\ \mathrm{PW}_m^{\mathrm{eq},1} &= \frac{1}{\mathrm{PEP}_m} \int_{\mathbb{R}} P_m(t - \Delta t) b_m(t) dt. \end{aligned} \qquad (20)$$

In (20), $b_m(t)$ represents the temporal blanker generated by the received composite pulse. Following the RTCA DO-292 blanker model [1], $b_m(t)$ is expressed as, from (13),

$$b_m(t) = \begin{cases} 0 \text{ if } t \in I_{bdc,m} \\ 1 \text{ otherwise} \end{cases} \qquad (21)$$

Note that $b_m(t)$ is an artificial signal since only one DME/TACAN source is considered to trigger the blanker, whereas in reality, all sources can trigger the blanker [7]. Nevertheless, the impact of the other sources has already been accounted for in (17) and is approximated to $(1 - bdc)$ [7].

Using $I_{bdc,m}$ expression (13) and assuming that the blanked interval $I^0_{\mathrm{bdc},m}$ ($I^1_{\mathrm{bdc},m}$) generated by the first (second) pulse impact on the second (first) pulse is negligible given the 12 µs separation [1], $\mathrm{PW}_m^{\mathrm{eq},0}$ and $\mathrm{PW}_m^{\mathrm{eq},1}$ are given by

$$\begin{aligned} \mathrm{PW}_m^{\mathrm{eq},0} &= \int_{\mathbb{R}} e^{-\alpha t^2} dt - \int_{t \in I^0_{\mathrm{bdc},m}} e^{-\alpha t^2} dt \\ \mathrm{PW}_m^{\mathrm{eq},1} &= \int_{\mathbb{R}} e^{-\alpha (t-\Delta t)^2} dt - \int_{t \in I^1_{\mathrm{bdc},m}} e^{-\alpha (t-\Delta t)^2} dt \end{aligned} \qquad (22)$$

A closed-form solution of (22) can be found by considering the two following cases:

1. Received PEP of beacon m pulses are below-blanker. Then, $I_{\mathrm{bdc},m} = \{\emptyset\}$ and, by solving the Gaussian integral,

$$\begin{aligned} \mathrm{PW}_m^{\mathrm{eq},0} &= \int_{\mathbb{R}} e^{-\alpha t^2} dt = \sqrt{\pi/\alpha} \\ \mathrm{PW}_m^{\mathrm{eq},1} &= \int_{\mathbb{R}} e^{-\alpha (t-\Delta t)^2} dt = \sqrt{\pi/\alpha} \\ \mathrm{PW}_m^{\mathrm{eq}} &= \mathrm{PW}_m^{\mathrm{eq},0} + \mathrm{PW}_m^{\mathrm{eq},1} = 2\sqrt{\pi/\alpha} \end{aligned} \qquad (23)$$

2. Received PEP of beacon m pulses are above-blanker. Then $\mathrm{PW}_m^{\mathrm{pulse}}$ is given by

$$
\begin{aligned}
\mathrm{PW}_m^{\mathrm{eq},0} &= \int_{\mathbb{R}} e^{-\alpha t^2} dt - \int_{\mathrm{l}_m^0}^{\mathrm{r}_m^0} e^{-\alpha t^2} dt \\
&= \sqrt{\frac{\pi}{\alpha}} \operatorname{erfc}\left(\sqrt{\alpha} w_m\right), \\
\mathrm{PW}_m^{\mathrm{eq},1} &= \int_{\mathbb{R}} e^{-\alpha (t-\Delta t)^2} dt - \int_{\mathrm{l}_m^1}^{\mathrm{r}_m^1} e^{-\alpha (t-\Delta t)^2} dt \\
&= \sqrt{\frac{\pi}{\alpha}} \operatorname{erfc}\left(\sqrt{\alpha} w_m\right), \\
\mathrm{PW}_m^{\mathrm{eq}} &= \mathrm{PW}_m^{\mathrm{eq}} + \mathrm{PW}_m^{\mathrm{eq}} = 2\sqrt{\frac{\pi}{\alpha}} \operatorname{erfc}\left(\sqrt{\alpha} w_m\right),
\end{aligned}
\tag{24}
$$

where erfc is the complementary error function,

$$
\operatorname{erfc}(x) = \frac{2}{\sqrt{\pi}} \int_x^{\infty} e^{-t^2} dt \,. \tag{25}
$$

From the definition of R_{I}, $\mathrm{PW}_m^{\mathrm{eq}}$ is the most important parameter as it will need to be updated with the introduction of MP.

Note that R_{I} definition (17) provided in this paper slightly differs from the one proposed in [1]. This is because the post-blanker RFI power spectrum density (PSD) used in the SSC term is assumed not to be perfectly spread as it is shown in [7], better modelling R_{I}, contrary to the assumption of [1]. However, since the only modification assumed in this paper by the introduction of MP is for the formula of $\mathrm{PW}_m^{\mathrm{eq}}$, both models from [1] and [7] are modified in the same manner.

III. STATISTICAL C/N_0 DEGRADATION MODEL CONSIDERING MULTIPATH

In this section, the current MP-free statistical C/N_0 degradation model is updated to account for echoes generated by scatterers in the Radio Line Of Sight (RLOS) of the DME/TACAN beacons. The term "echo" or "MP" are used in the same way to designate multipath. The proposed model aims at providing an average value of the C/N_0 degradation for a single point of an aircraft trajectory and is thus statistical. The MP collisions are tackled by the model and the models of PW (and thus R_{I}) and pw (and thus bdc) are updated to accurately consider MP.

A. Received Signal Model Under the Statistical Assumption Considering Multipath

Considering MP, the main difference for the received signal is that the received composite pulse is no more composed of one pair of pulses but of N_m pair of pulses, where $N_m \geq 1$ and N_m is the number of scatterers in the RLOS of the DME/TACAN beacon. In that case, the expression of the received signal $r(t)$ (2) at the output of the blanker is updated into, still considering a single aircraft position,

$$
\begin{aligned}
r(t) = \sum_{m=1}^{M} \sum_{\kappa=1}^{\mathrm{K}_m} \sum_{n=0}^{N_m} A_m^n s_{\mathrm{bb}}(t - t_m^\kappa - \tau_m^n) \cdot \\
\cos\left(2\pi \left(f_m + f_{D,m}^n\right) t + \theta_m^{\kappa,n}\right) b_m(t - t_m^\kappa - \tau_m^0),
\end{aligned}
\tag{26}
$$

where the index $n = 0$ is associated with the direct (LOS) composite pulse.

For this section (and this section only), it is more convenient to express each received composite pulse κ with the individual Gaussian pulses $g(t)$ (1) considering that the second pulse of the MP-free composite pulse is also an echo. In that case, the received composite pulse is composed of $N_m^{\mathrm{p}} + 1$ Gaussian pulses where N_m^{p} is the number of echoed pulses, $N_m^{\mathrm{p}} = 2N_m + 1$. Under this rationale, $r(t)$ is expressed in its most conceived manner as

$$
\begin{aligned}
r(t) = \sum_{m,\kappa,n} f(m,\kappa,n), \\
f(m,\kappa,n) = A_m^n g(t - t_m^\kappa - \tau_m^n) \cdot \\
\cos\left(2\pi \left(f_m + f_{D,m}^n\right) t + \theta_m^{\kappa,n}\right) b_m(t - t_m^\kappa - \tau_m^0),
\end{aligned}
\tag{27}
$$

where $m \in [\![1, M]\!]$, $\kappa \in [\![1, \mathrm{K}_m]\!]$ and $n \in [\![0, N_m^p]\!]$. Note that, with this rationale, there always exists an n such that $\tau_m^n = \Delta t$.

The function $b_m(t)$ represents the temporal blanker triggered by a received composite pulse. The function b_m is simply delayed to match with the time of reception of the composite pulses but is always the same: since the aircraft is not moving, the received composite pulse is always the same, i.e., the additional delay of the echoes with respect to the LOS is the same no matter t_m^κ. Note that this modelling also assumes that the blanker is only triggered by source m and not by other sources $m' \neq m$ [7].

The parameters A_m^n, τ_m^n, $f_{D,m}^n$ are the amplitude, delay, Doppler frequency of pulse n of beacon m, respectively. Furthermore, the additional phase $\theta_m^{\kappa,n}$ (5) is updated into

$$
\theta_m^{\kappa,n} = \theta_{0,m}^{\kappa} + \theta_{\mathrm{D},m}^n + \theta_{\mathrm{e},m}^n \bmod 2\pi. \tag{28}
$$

where $\theta_{\mathrm{D},m}^n$ is the additional phase due to initial propagation time delay of pulse n, i.e., $\theta_{\mathrm{D},m}^n = -2\pi f_m \tau_m^n$. Since MP are now considered, the additional phase offset $\theta_{\mathrm{e},m}^n$ introduced by any physical effects generated by the environment must now also account for reflections and thus not only the weather but also any temporal properties of the scatterer (constructions, closed shutters, open windows etc.) must be considered. Since MP are generated from different scatterers, $\theta_{\mathrm{e},m}^n$ now depends on n.

Assuming a single point of an aircraft trajectory, environmental conditions and scatterers properties can be

assumed unknown, and thus $\theta^n_{\mathrm{e},m}$ is modelled as a uniform distribution over $[0,2\pi)$, independent for different beacon ($m \neq m'$) and scatterers ($n \neq n'$). This assumption is referred as the statistical assumption in this article.

To summarize, the three random variables of $r(t)$ are modelled as

$$\begin{aligned} t^\kappa_m &\sim U[0,T_0],\ t^\kappa_m \perp \theta^{\kappa',n}_{m'}\ \forall\, m,m',\kappa,\kappa',n, \\ \theta^\kappa_{0,m} &\sim U[0,2\pi),\ \theta^\kappa_{0,m} \perp \theta^{\kappa'}_{0,m'},\ \forall \binom{m}{\kappa} \neq \binom{m'}{\kappa'}, \\ \theta^n_{\mathrm{e},m} &\sim U[0,2\pi),\ \theta^n_{\mathrm{e},m} \perp \theta^{n'}_{\mathrm{e},m'},\ \forall \binom{m}{n} \neq \binom{m'}{n'}, \\ \theta^n_{\mathrm{e},m} &\perp \theta^\kappa_{0,m'}\ \forall\, m,m',\kappa,n. \end{aligned} \tag{29}$$

B. Average Power of the Received Signal at Blanker Output

It is necessary to derive the average power P^s_r of the post blanker received signal $r(t)$ in presence of echoes in order to update the formulas of bdc and R_I under the statistical assumption. As a random and real signal, the average received power P^s_r of $r(t)$ under the statistical assumption is given by

$$P^s_\mathrm{r} = \lim_{T\to\infty} \frac{1}{2T} \int_{-T}^{T} E[r(t)^2]dt. \tag{30}$$

Note that in the integral of (30), a change of the value of t in the integral does not represent a change of the aircraft position (the aircraft is always fixed to a trajectory), but rather all the possible instants where the aircraft is in its fixed trajectory. Since these instants can happen anytime and are equally likely, the integral is weighted by a factor $1/2T$ where T tends toward infinite.

The expectation $E[r(t)^2]$ can be expressed as, following (27),

$$\begin{aligned} E[r(t)^2] &= E\left[\left(\sum_{m,\kappa,n} f(m,\kappa,n)\right)^2\right] \\ &= \sum_{m,m',\kappa,\kappa',n,n'} E[f(m,\kappa,n)f(m',\kappa',n')] \end{aligned} \tag{31}$$

by the linearity of the expectation. Let E_f be $E[f(m,\kappa,n)f(m',\kappa',n')]$. Then, since $t^\kappa_m \perp \theta^{\kappa,n}_m$,

$$E_f = A^n_m A^{n'}_{m'} E^\mathrm{b}_g E_\mathrm{cos} \tag{32}$$

where

$$\begin{aligned} E^\mathrm{b}_g &= E[g(t-t^\kappa_m-\tau^n_m)g\left(t-t^{\kappa'}_{m'}-\tau^{n'}_{m'}\right)\cdot \\ &\quad b_m\big(t-t^\kappa_m-\tau^0_m\big)b_{m'}(t-t^{\kappa'}_{m'}-\tau^0_{m'})] \\ E_\mathrm{cos} &= E[\cos\big(2\pi\big(f_m+f^n_{D,m}\big)t+\theta^{\kappa,n}_m\big)\cdot \\ &\quad \cos\left(2\pi\left(f_{m'}+f^{n'}_{D,m'}\right)t+\theta^{\kappa',n'}_{m'}\right)] \end{aligned} \tag{33}$$

The value of E_f is investigated regarding the triplets (m,κ,n) and (m',κ',n'):

1. Assume emitting sources to be different, i.e., $m \neq m'$ then $\theta^\kappa_{0,m} \perp \theta^{\kappa'}_{0,m'}$, $\theta^n_{\mathrm{r},m} \perp \theta^{n'}_{\mathrm{r},m'}$ and thus E_cos can be separated into two expectations that both equal 0 by the law of total expectation since $\theta^\kappa_{0,m}$ and $\theta^n_{\mathrm{r},m}$ are uniform on $[0,2\pi)$. Thus, if $m \neq m'$ then $E_f = 0$.
2. Assume emitting sources are the same ($m = m'$) but emitted pulses come from different pairs, i.e., $\kappa \neq \kappa'$. Then, if $n = n'$, the product of the two gaussian pulses in E^b_g is assumed to be zero since pulse pair are at least separated by 60 µs as specified in [10]. If $n \neq n'$, the product of the two gaussian pulses is still zero since MP having an additional delay close to 60 µs are expected to have an extremely small PEP (see numerical results in [8]). Therefore, if $m = m'$ and $\kappa \neq \kappa'$ then $E_f = 0$.
3. Assume emitted pairs of the same emitting source ($m = m'$ and $\kappa = \kappa'$) but different echoes, i.e., $n \neq n'$ then $\theta^n_{\mathrm{e},m} \perp \theta^{n'}_{\mathrm{e},m}$ and by the law of total expectation, assuming $\theta^\kappa_{0,m}$ known, $E_\mathrm{cos} = 0$ since $\theta^n_{\mathrm{e},m}$ and $\theta^{n'}_{\mathrm{e},m} \sim U[0,2\pi)$. Thus, if $m = m'$, $\kappa = \kappa'$ and $n \neq n'$ then $E_f = 0$.

To conclude, E_f is not zero only if $m = m'$, $\kappa = \kappa'$ and $n = n'$. Thus,

$$P^s_\mathrm{r} = \lim_{T\to\infty} \frac{1}{2T} \int_{-T}^{T} \sum_{m,\kappa,n} E[f(m,\kappa,n)^2]dt\,. \tag{34}$$

The complete derivation of (34) is conducted in Appendix A. Final expression of P^s_r is given by

$$P^s_\mathrm{r} = \sum_{m,n} \mathrm{PRF_m PEP}^n_m \int_{-\infty}^{\infty} e^{-\alpha(u-\tau^n_m)^2} b_m(u-\tau^0_m)du\,. \tag{35}$$

Finally, all the cross terms of equation (31) are null and thus the pulses contributions can be investigated independently for the new $\mathrm{pw}^\mathrm{eq}_m$ and $\mathrm{PW}^\mathrm{eq}_m$ formulas. In this paper, pulses are said independent if the power of their sum is equal to the sum of their powers, even if they collide. The derivation of $\mathrm{pw}^\mathrm{eq}_m$ and $\mathrm{PW}^\mathrm{eq}_m$ considering MP is provided in Section III.C and III.D, respectively.

C. $\mathrm{pw}^\mathrm{eq}_m$ Mathematical Model Considering Multipath

In this section, the mathematical expression of $\mathrm{pw}^\mathrm{eq}_m$ (12) is updated to accurately account for echoed pulses.

With the introduction of echoes, the received composite pulse is no longer constituted of two disjoint Gaussian pulses but is composed of the LOS and the MP, that can potentially collide. Therefore, considering MP, $I_{\mathrm{bdc},m}$, the blanked interval

generated by one received composite pulse must account for the blanked intervals generated by the echoed pulses.

As for the MP-free case, $\mathrm{pw}_m^{\mathrm{eq}}$ is still invariant by translation, and therefore the delay of the first received pulse $t_m^{\kappa_0} + \tau_m^0$ can be chosen at 0 to simplify the derivations. Fig. 4 provides a graphical example of the blanked intervals generated by a direct pulse (in red) received at $t_m^{\kappa_0} + \tau_m^0 = 0$ and an echoed pulse (in green) above-threshold, where the blanked interval generated by the echo must clearly be accounted for.

Therefore, in presence of echoes, $I_{\mathrm{bdc},m}$ is updated from (13) into

$$I_{\mathrm{bdc},m} = \bigcup_{n=0}^{N_m^{\mathrm{p}}} I_{\mathrm{bdc},m}^n, \tag{36}$$

where $I_{\mathrm{bdc},m}^n$ is the blanked interval generated by echo n and is expressed as

$$\begin{aligned} I_{\mathrm{bdc},m}^n &= \begin{cases} \{\emptyset\} \text{ if } \mathrm{PEP}_m^n \le \mathrm{T_H} \\ [\mathrm{l}_m^n, \mathrm{r}_m^n] \text{ otherwise,} \end{cases} \\ &\begin{cases} \mathrm{l}_m^n = \tau_m^n - w_m^n \\ \mathrm{r}_m^n = \tau_m^n + w_m^n, \end{cases} \\ w_m^n &= \sqrt{\ln\left(\frac{\mathrm{PEP}_m^n}{\mathrm{T_H}}\right)/\alpha}, \end{aligned} \tag{37}$$

where $\mathrm{PEP}_m^n = (A_m^n)^2/2$ is the PEP of echo n with respect to beacon m. Note that equation (36) is only valid because the power of the sum is equal to the sum of power under the statistical assumption.

Furthermore, it is more convenient to express pw_m only with disjoint blanked intervals since some $I_{\mathrm{bdc},m}$ may overlap. Let $B_{\mathrm{d},m}^q$ be the disjoint blanked intervals and Q_m the number of disjoint blanked intervals generated by source m, then

$$\begin{aligned} I_{\mathrm{bdc},m} &= \coprod_{q=1}^{Q_m} B_{\mathrm{d},m}^q \\ B_{\mathrm{d},m}^q &= [\mathrm{l}_{\mathrm{d},m}^q, \mathrm{r}_{\mathrm{d},m}^q]. \end{aligned} \tag{38}$$

The bounds $\mathrm{l}_{\mathrm{d},m}^q$ and $\mathrm{r}_{\mathrm{d},m}^q$ of $B_{\mathrm{d},m}$ can be retrieved recursively using $I_{\mathrm{bdc},m}^n$, ordering the l_m^n such that $\mathrm{l}_m^n \le \mathrm{l}_m^{n+1}$, as:

$$\begin{aligned} \mathrm{l}_{\mathrm{d},m}^1 &= \mathrm{l}_m^1, \\ \mathrm{r}_{\mathrm{d},m}^1 &= \mathrm{comp}\left(\mathrm{r}_m^1, \mathrm{l}_m^2\right), \\ \mathrm{l}_{\mathrm{d},m}^q &= \min_n\left(\mathrm{l}_m^n | \mathrm{l}_m^n > \mathrm{l}_{\mathrm{d},m}^{q-1}\right), q \ge 1, \\ n_q &= \arg\left(\min_n\left(\mathrm{l}_m^n | \mathrm{l}_m^n > \mathrm{l}_{\mathrm{d},m}^{q-1}\right)\right), q \ge 1, \\ \mathrm{r}_{\mathrm{d},m}^q &= \mathrm{comp}\left(\mathrm{r}_m^{n_q}, \mathrm{l}_m^{n_q+1}\right), \end{aligned} \tag{39}$$

$$\begin{aligned} &\mathrm{comp}\left(\mathrm{r}_m^n, \mathrm{l}_m^{n+1}\right) \\ &= \begin{cases} \mathrm{r}_m^n \text{ if } \mathrm{r}_m^n \le \mathrm{l}_m^{n+1} \\ \mathrm{comp}\left(\max\left(\mathrm{r}_m^n, \mathrm{r}_m^{n+1}\right), \mathrm{l}_m^{n+2}\right) \text{ otherwise.} \end{cases} \end{aligned}$$

Finally, in presence of MP, $\mathrm{pw}_m^{\mathrm{eq}}$ is updated from (16) into, by the σ-additivity of μ,

$$\begin{aligned} \mathrm{pw}_m^{\mathrm{eq}} &= \mu\left(\coprod_{q=1}^{Q_m} B_{\mathrm{d},m}^q\right) \\ &= \sum_{q=1}^{Q_m} \mu\left(B_{\mathrm{d},m}^q\right) = \sum_{q=1}^{Q_m} \left(\mathrm{r}_{\mathrm{d},m}^q - \mathrm{l}_{\mathrm{d},m}^q\right). \end{aligned} \tag{40}$$

Therefore, in presence of MP, bdc from (11) is simply updated by using the expression (40) of $\mathrm{pw}_m^{\mathrm{eq}}$. Fig. 4 provides a graphical representation of the union of the overlapping $I_{\mathrm{bdc},m}^0$ and $I_{\mathrm{bdc},m}^1$ overlapping blanked intervals from the direct (in red) and the echoed pulses (in green), to generate one disjoint blanked interval $B_{\mathrm{d},m}^1$.

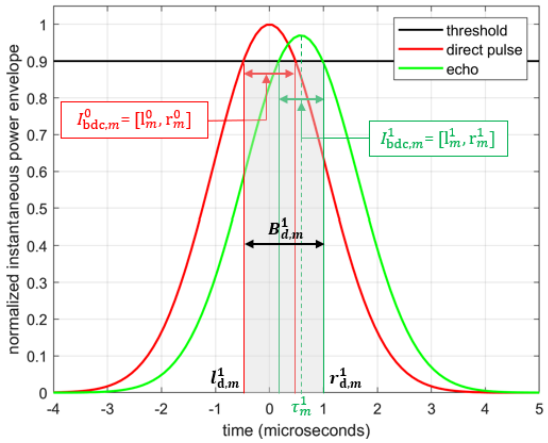

Fig. 3. Graphical representation of the overlapping blanked intervals generated by the direct pulse (in red) with an echoed pulse (in green) and the resulting disjoint blanked interval (in grey) at the output of the algorithm (39).

D. $\mathrm{PW}_m^{\mathrm{eq}}$ Mathematical Model Considering Multipath

In this subsection, the mathematical expressions of $\mathrm{PW}_m^{\mathrm{eq}}$ (19) is updated to accurately account for echoes. First, an additional assumption is made on the impact of blanked interval on different received composite pulse κ and κ' with $\kappa \neq \kappa'$. Then, the expression of $\mathrm{PW}_m^{\mathrm{eq}}$ is provided based on the expression of the average post-blanker received power (35). Finally, a closed form of $\mathrm{PW}_m^{\mathrm{eq}}$ is obtained accounting for the three possible scenarios, by means of erfc functions.

Pair independence assumption: It is assumed that the blanking interval applied to a composite pulse κ of source m is

not affected by any other composite pulse $\kappa' \neq \kappa$ of the same source m. This is because composite pulses are at least separated by 60 µs [10] and that echoed pulses from pulse κ are very unlikely to trigger the threshold when they arrive close enough to composite pulse κ', with $\kappa' > \kappa$ (see numerical results in [8]) to have any impact on the PW of composite pulse κ'.

Update of $\mathrm{PW}_m^{\mathrm{eq}}$ *considering multipath:* In presence of MP, the mathematical expression of $\mathrm{PW}_m^{\mathrm{eq}}$ is retrieved from (18) and from the expression of the average post blanker received power (35) as

$$\begin{aligned} P_{\mathrm{r}}^{\mathrm{s}} &= \sum_{m=1}^{M} P_{\mathrm{r},m}^{\mathrm{s}}, \\ P_{\mathrm{r},m}^{\mathrm{s}} &= \mathrm{PEP}_m^0 \mathrm{PW}_m^{eq} \mathrm{PRF}_m, \\ \mathrm{PW}_m^{eq} &= \sum_{n=0}^{N_m^{\mathrm{p}}} \frac{\mathrm{PEP}_m^n}{\mathrm{PEP}_m^0} \mathrm{PW}_m^{\mathrm{eq},n}, \end{aligned} \tag{41}$$

where $\mathrm{PW}_m^{\mathrm{eq},n}$ is the equivalent pulse width whose energy in the same of the energy post-blanker echo n relatively to beacon m, i.e.,

$$\mathrm{PW}_m^{\mathrm{eq},n} = \int_{-\infty}^{\infty} e^{-\alpha(t-\tau_m^n)^2} b_m(t-\tau_m^0)dt\,. \tag{42}$$

As for the MP-free case, $\mathrm{PW}_m^{\mathrm{eq},n}$ is translation invariant and therefore $t_m^\kappa + \tau_m^0$ can be chosen equal to 0, which is equivalent to say that both $t_m^\kappa = 0$ and $\tau_m^0 = 0$ since the two quantities are positives. In that case $I_{\mathrm{bdc},m}$ in the MP case from (38) can be used and

$$\begin{aligned} \mathrm{PW}_m^{\mathrm{eq},n} &= \int_{\mathbb{R}} e^{-\alpha(t-\tau_m^n)^2} dt - \int_{t\in I_{\mathrm{bdc},m}} e^{-\alpha(t-\tau_m^n)^2} dt \\ &= \sqrt{\pi/\alpha} - \sum_{q}^{Q_m} J_m^{n,q}\,, \end{aligned} \tag{43}$$

As the $B_{\mathrm{d},m}^q$ are disjoints. Therefore, the intervals $J_m^{n,q}$ are expressed as

$$\begin{aligned} J_m^{n,q} &= \int_{t\in B_{\mathrm{d},m}^q} e^{-\alpha(t-\tau_m^n)^2} dt = \int_{\mathrm{l}_{\mathrm{d},m}^q}^{\mathrm{r}_{\mathrm{d},m}^q} e^{-\alpha(t-\tau_m^n)^2} dt \\ &= \int_{\mathrm{l}_{\mathrm{d},m}^q}^{\infty} e^{-\alpha(t-\tau_m^n)^2} dt - \int_{\mathrm{r}_{\mathrm{d},m}^q}^{\infty} e^{-\alpha(t-\tau_m^n)^2} dt \\ &= \frac{\sqrt{\pi/\alpha}}{2} \begin{pmatrix} \mathrm{erfc}\left(\sqrt{\alpha}\left(\mathrm{l}_{\mathrm{d},m}^q - \tau_m^n\right)\right) - \\ \mathrm{erfc}\left(\sqrt{\alpha}\left(\mathrm{r}_{\mathrm{d},m}^q - \tau_m^n\right)\right) \end{pmatrix}. \end{aligned} \tag{44}$$

The sign of $\mathrm{l}_{\mathrm{d},m}^q - \tau_m^n$ and $\mathrm{r}_{\mathrm{d},m}^q - \tau_m^n$ varies according to three possible scenario that are detailed below.

Scenario 1: Echo n is being blanked by disjoint blanked interval q in its center, i.e., $\tau_m^n \in B_{\mathrm{d},m}^q$. A graphical representation of this scenario is provided in Fig. 5, where (red) echo n is blanked at its center by the disjoint interval generated by another (green) echo.

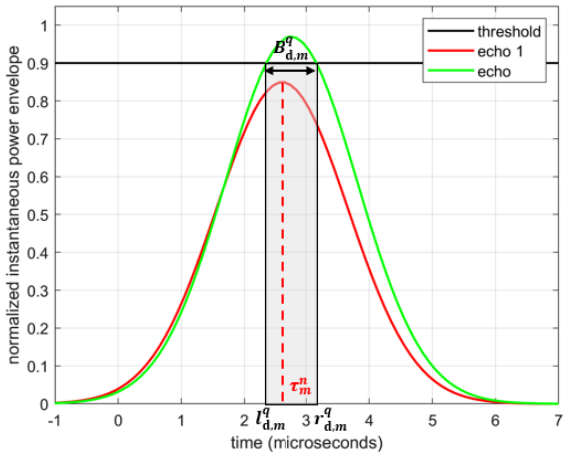

Fig. 4. Graphical representation of scenario 1: (red) echo n is being blanked at its center by the disjoint blanked interval generated by another (green) echo.

Note that this scenario differs from the MP-free case (24) since $B_{\mathrm{d},m}^q$ is not necessarily centered in t_m^κ. In that case, $\mathrm{l}_{\mathrm{d},m}^q - \tau_m^n \leq 0$ and $\mathrm{r}_{\mathrm{d},m}^q - \tau_m^n \geq 0$. Therefore, since $\mathrm{erfc}(-x) = 2 - \mathrm{erfc}(x)$, $J_m^{n,q}$ is expressed as, using the absolute value for convenience and from (44)

$$J_m^{n,q} = \frac{\sqrt{\pi/\alpha}}{2} \begin{pmatrix} 2 - \mathrm{erfc}\left(\sqrt{\alpha}\left|\mathrm{l}_{\mathrm{d},m}^q - \tau_m^n\right|\right) - \\ \mathrm{erfc}\left(\sqrt{\alpha}\left|\mathrm{r}_{\mathrm{d},m}^q - \tau_m^n\right|\right) \end{pmatrix}. \tag{45}$$

Scenario 2: Echo n is being blanked by disjoint blanked interval q on its left side, i.e., $\tau_m^n > r_{\mathrm{d},m}^q$. A graphical representation of this scenario is provided in Fig. 6, where (red) echo n is blanked on its left side by the disjoint interval generated by another (green) echo.

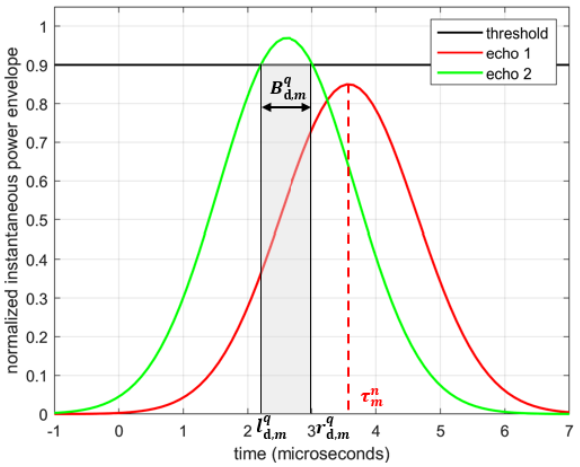

Fig. 5. Graphical representation of scenario 1: (red) echo n is being blanked by the disjoint blanked interval generated by another (green) echo on its left side.

In this scenario, $\mathrm{l}_{\mathrm{d},m}^{q} - \tau_m^n < 0$ and $\mathrm{r}_{\mathrm{d},m}^{q} - \tau_m^n < 0$. Therefore, in scenario 2,

$$J_m^{n,q} = \frac{\sqrt{\pi/\alpha}}{2}\begin{pmatrix}\mathrm{erfc}\left(\sqrt{\alpha}\left|\mathrm{r}_{\mathrm{d},m}^{q} - \tau_m^n\right|\right) - \\ \mathrm{erfc}\left(\sqrt{\alpha}\left|\mathrm{l}_{\mathrm{d},m}^{q} - \tau_m^n\right|\right)\end{pmatrix}. \tag{46}$$

Scenario 3: Echo n is being blanked by disjoint blanked interval q on its right side, i.e., $\tau_m^n < l_{\mathrm{d},m}^{q}$. A graphical representation of this scenario is provided in Fig. 6, where (red) echo n is blanked on its right side by the disjoint interval generated by another (green) echo.

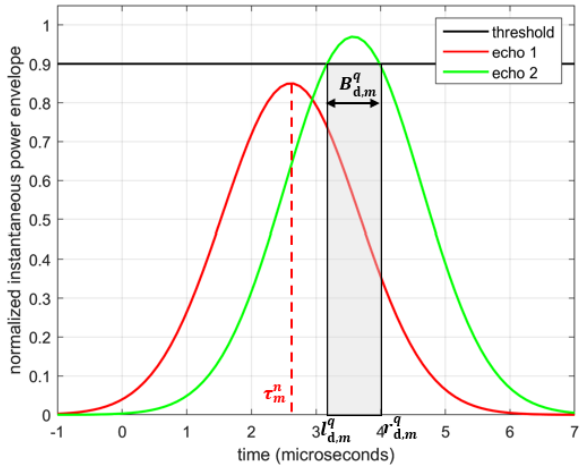

Fig. 6 Graphical representation of scenario 1: (red) echo n is being blanked by the disjoint blanked interval generated by another (green) echo on its right side.

In this scenario, $\mathrm{l}_{\mathrm{d},m}^{q} - \tau_m^n > 0$ and $\mathrm{r}_{\mathrm{d},m}^{q} - \tau_m^n > 0$. Therefore, in scenario 3,

$$J_m^{n,q} = \frac{\sqrt{\pi/\alpha}}{2}\begin{pmatrix}\mathrm{erfc}\left(\sqrt{\alpha}\left|\mathrm{l}_{\mathrm{d},m}^{q} - \tau_m^n\right|\right) - \\ \mathrm{erfc}\left(\sqrt{\alpha}\left|\mathrm{r}_{\mathrm{d},m}^{q} - \tau_m^n\right|\right)\end{pmatrix}. \tag{47}$$

The three formulas obtained for $J_m^{n,q}$ from the three scenarios can be reunited into one equation using the indicator $\mathbf{1}_E(x)$ and the $\mathrm{sign}(x)$ functions. In that case, $\mathrm{PW}_m^{\mathrm{eq,n}}$ from (43) is expressed as

$$\mathrm{PW}_m^{\mathrm{eq,n}} = \frac{\sqrt{\pi/\alpha}}{2}\Bigg\{2 - \sum_{q=1}^{Q_m}\begin{bmatrix}2\cdot\mathbf{1}_{B_{\mathrm{d},m}^{q}}(\tau_m^n) - \\ \mathrm{sign}\left(\tau_m^n - l_{\mathrm{d},m}^{q}\right)\mathrm{erfc}\left(\sqrt{\alpha}\left|\mathrm{l}_{\mathrm{d},m}^{q} - \tau_m^n\right|\right) - \\ \mathrm{sign}\left(r_{\mathrm{d},m}^{q} - \tau_m^n\right)\mathrm{erfc}\left(\sqrt{\alpha}\left|r_{\mathrm{d},m}^{q} - \tau_m^n\right|\right)\end{bmatrix}\Bigg\}. \tag{48}$$

Furthermore, since $\sum_{q=1}^{Q_m}\mathbf{1}_{B_{\mathrm{d},m}^{q}}(\tau_m^{\kappa,n}) = \mathbf{1}_{I_{\mathrm{bdc},m}}(\tau_m^n)$, the final expression of $\mathrm{PW}_m^{\mathrm{eq,n}}$ is expressed as

$$\mathrm{PW}_m^{\mathrm{eq,n}} = \frac{\sqrt{\pi/\alpha}}{2}\Bigg\{2\left(1 - \mathbf{1}_{I_{\mathrm{bdc},m}^{\kappa}}(\tau_m^n)\right) + \sum_{q=1}^{Q_m}\begin{bmatrix}\mathrm{sign}\left(\tau_m^n - l_{\mathrm{d},m}^{q}\right)\mathrm{erfc}\left(\sqrt{\alpha}\left|\mathrm{l}_{\mathrm{d},m}^{q} - \tau_m^{\kappa,n}\right|\right) + \\ \mathrm{sign}\left(r_{\mathrm{d},m}^{q} - \tau_m^n\right)\mathrm{erfc}\left(\sqrt{\alpha}\left|r_{\mathrm{d},m}^{q} - \tau_m^{\kappa,n}\right|\right)\end{bmatrix}\Bigg\}. \tag{49}$$

And R_{I} is updated in the presence of MP by using the expression (49) of $\mathrm{PW}_m^{\mathrm{eq,n}}$.

Note that for R_{I}, it is assumed that the SSC is the same for each received pulses (MP or LOS) independently of the addition instant of times blanked due to the introduction of MP for simplification purposes. The study of the variations of SSC in that case are out of the scope of this paper and left for future work.

E. Validation of the Average Received Power Formula Under the Statistical Assumption

Formula of the post-blanker average received power (41) using the expression of $\mathrm{PW}_m^{\mathrm{eq,n}}$ provided in (49) is validated by means of Monte-Carlo simulations.

The objective of the Monte-Carlo simulation under the statistical assumption is to provide a validation matrix $(\mathrm{V})_{(\tau^1,\tau^2)}$ where each element of V is the ratio (in dB) of the average received power computed by the Monte-Carlo simulation, $P_{\mathrm{r}}^{\mathrm{s,MC}}$, with the received power formula $P_{\mathrm{r}}^{\mathrm{s}}$ provided in (41) and (49), i.e.,

$$(\mathrm{V})_{(\tau^1,\tau^2)} = 10\log_{10}\left(\frac{P_{\mathrm{r,MC}}^{\mathrm{s}}(\tau^1,\tau^2)}{P_{\mathrm{r}}^{\mathrm{s}}(\tau^1,\tau^2)}\right) \tag{50}$$

To derive the matrix V, a single DME beacon and two multipath ($M = 1$, $N_m = 2$ and $N_m^{\mathrm{p}} = 5$) with PEP above the blanking threshold ($\mathrm{T_H} = -120$ dBW) are considered. Since only one beacon and one emission are considered, the sub-index m and the upper-index κ are discarded. The deterministic and random parameters of the Monte-Carlo simulation are summarized in the first column of Table I. The value of τ^0 is not indicated since τ^0 is considered equal to 0. The number of Monte-Carlo simulations per combination of pair pulse deterministic parameters is referred as N_{MC}.

Table I
Parameters definition for the Monte-Carlo simulations under the statistical and fixed environment assumptions. The sub-index m is discarded since only one beacon ($M = 1$) is considered.

		Statistical Section III.E	Fixed Environment Section IV.C
Deterministic Parameters	N_{MC}	10 000	10 000
	N_m	2	1
	T_0 (ms)	-	20
	K	1	54
	PEP^n (dBW)	{-118, -118, -118}	{-121, -121}
	τ^1 (μs)	$\in$ [0,22] Step = 0.4	$\in$ [0,22] Step = 1
	τ^2 (μs)	$\in$ [0,22] Step = 0.4	-
	θ_{e}^n	-	$\in [0,2\pi)^2$
Random Parameters	X	$X^{\mathrm{s}} = \begin{pmatrix} \theta_0 \\ \theta_r^0 \\ \theta_r^1 \\ \theta_r^2 \end{pmatrix}$	$X^{\mathrm{fe}} = \begin{pmatrix} t^1 \\ \vdots \\ t^{\mathrm{K}} \\ \theta_0^1 \\ \vdots \\ \theta_0^{\mathrm{K}} \end{pmatrix}$

For each pair (τ^1, τ^2), N_{MC} draws of the vector X^{s} are realized. For one draw ι, $\iota \in [\![0, N_{\mathrm{MC}}]\!]$ of the random vector X_ι^{s} and the deterministic parameters, the complex representation $r_\iota^{\mathrm{ce}}(t)$ of $r_\iota(t)$ is obtained such that $r_\iota(t) = Re\left(r_\iota^{\mathrm{ce}}(t)\right)$ and

$$r_\iota^{\mathrm{ce}}(t) = \sum_{n=0}^{N_m} A^n s_{\mathrm{bb}}(t - \tau^n) e^{-j2\pi(\theta_{0,\iota} + \theta_{r,\iota}^n)} b(t). \qquad (51)$$

Using $r^{\mathrm{ce}}(t)$, one $P_{\mathrm{r,MC}}^{\mathrm{s},\iota}$, $\iota \in [\![0, N_{\mathrm{MC}}]\!]$ is obtained through simulation by integrating $|r^{\mathrm{ce}}(t)|^2$ by means of the trapeze MATLAB integration method. Finally, the Monte-Carle average post-blanker received power $P_{\mathrm{r,MC}}^{\mathrm{s}}(\tau^1, \tau^2)$ by averaging the $P_{\mathrm{r,MC}}^{\mathrm{s},\iota}$, i.e.,

$$\begin{aligned} P_{\mathrm{r,MC}}^{\mathrm{s},\iota}(\tau^1, \tau^2) &= \int_{-\infty}^{\infty} |r_\iota^{\mathrm{ce}}(t)|^2 dt \\ P_{\mathrm{r,MC}}^{\mathrm{s}}(\tau^1, \tau^2) &= \frac{1}{N_{\mathrm{MC}}} \sum_{\iota=1}^{N_{\mathrm{MC}}} P_{\mathrm{r,MC}}^{\mathrm{s},\iota}(\tau^1, \tau^2). \end{aligned} \qquad (52)$$

The process is repeated for each possible pair (τ^1, τ^2) and the validation matrix V is provided in Fig. 3.

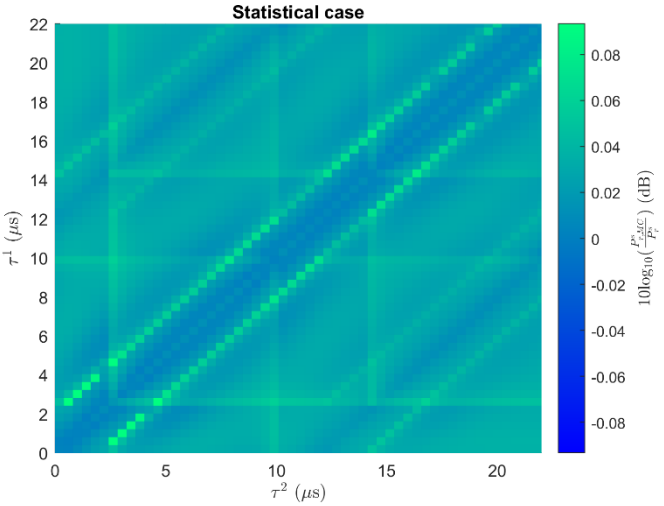

Fig. 7. Results of the Monte-Carlo simulations for the average received power P_r^s under the statistical assumption.

Fig. 3 shows that the ratio between $P_{\mathrm{r}}^{\mathrm{s}}$ (41) and $P_{\mathrm{r,MC}}^{\mathrm{s}}$ never exceed 0.08 dB and thus (35) is validated.

F. Model Necessary Inputs

To compute bdc (11) and R_{I} (17) in presence of MP, only the values of $\mathrm{pw}_m^{\mathrm{eq}}$ (40) and $\mathrm{PW}_m^{\mathrm{eq}}$ (49) updated for the presence of MP, are necessary. To derive these quantities, the precise knowledge of the blanked interval $I_{\mathrm{bdc},m}$ (38) is necessary. More specifically, the knowledge of the disjoint blanked intervals $B_{\mathrm{d},m}^q$ is mandatory and thus, the values of all w_m^n (37) must be known. Therefore, the values of all the additional delays τ_m^n and received PEP PEP_m^n must be determined in order compute R_{I}, bdc (40) and finally the C/N_0 degradation (10) in presence of MP.

Part II of this work addresses this requirement by proposing a complete propagation channel model specifically designed to provide τ_m^n and PEP_m^n for any MP generated by the scatterers in the RLOS of the visible DME/TACAN beacons [8].

IV. FIXED ENVIRONMENT C/N_0 DEGRADATION MODEL CONSIDERING MULTIPATH

In this section, the C/N_0 degradation model in presence of MP is investigated under the fixed environment assumption. First, the fixed environment assumption is provided. Second, the average post-blanker received power under the fixed-environment assumption is determined. Finally, applicability zones of the fixed environment model where closed-form of $\mathrm{PW}_m^{\mathrm{eq},n}$ and $\mathrm{pw}_m^{\mathrm{eq},n}$ can be found are provided.

Indeed, In that case, the formula of the average received power must be recalculated to see if the C/N_0 degradation model as proposed in Section III can still be used.

A. Fixed Environment Assumption

The fixed environment assumption is defined as short periods of time (i.e., less than a second) during an aircraft trajectory where environmental conditions can be assumed to be known and constant for short periods of time $[t, t+T_0]$ (i.e., less than a second) and therefore the phase offset produced by the physical effects generated by the environment is assumed to be deterministic, since scatterers or the weather are unlikely to change during T_0.

Therefore, under the fixed environment assumption, the phase offset $\theta_{\mathrm{r},m}^{n}$ introduced by the propagation channel due to any physical effects and reflections is assumed to be deterministic with a constant value during T_0, i.e., $\theta_{\mathrm{r},m}^{n} \in [0,2\pi)$. Furthermore, for a fixed source m, the difference between two additional delay τ_m^n and $\tau_m^{n'}$, $n \neq n'$ is assumed to be constant over $[t, t+T_0]$ since T_0 is very short.

Therefore, the received signal $r(t)$ under the fixed environment assumption is defined as

$$\begin{aligned} r(t) &= \sum_{m,\kappa,n} f(m,\kappa,n)\,, \\ f(m,\kappa,n) &= A_m^n s_{\mathrm{bb}}(t - t_m^\kappa - \tau_m^n)\cdot \\ &\quad \cos\left(2\pi\left(f_m + f_{D,m}^n\right)t + \theta_m^{\kappa,n}\right) b_m(t-\tau_m^0) \end{aligned} \tag{53}$$

where the random variables defined for the statistical assumption in (29) are updated into

$$\begin{aligned} t_m^\kappa &\sim U[0,T_0],\, t_m^\kappa \perp \theta_{m'}^{\kappa',n}\ \forall\, m,m',\kappa,\kappa',n, \\ \theta_{0,m}^\kappa &\sim U[0,2\pi),\, \theta_{0,m}^\kappa \perp \theta_{0,m'}^{\kappa'}\ \forall \binom{m}{\kappa} \neq \binom{m'}{\kappa'}, \\ \theta_{\mathrm{e},m}^n &\in [0,2\pi). \end{aligned} \tag{54}$$

Note that under the fixed environment assumption, pulse pair s_{bb} is used in for the received signal definition (instead of using the gaussian pulse g and considering the second pulse on a pair as an echo) and therefore the number of received MP is simply N_m. This approach simplifies the derivation of the average received power in that case.

B. Average Received Power at The Blanker Output

The derivation of the average received power in the fixed environment assumption $P_{\mathrm{r}}^{\mathrm{fe}}$ at the blanker output follows the exact same step as the derivation of $P_{\mathrm{r}}^{\mathrm{s}}$ under the statistical assumption as provided in Section III.B. The main difference is that under the fixed environment assumption, the expectation $E_{\cos}$ is not zero when $n \neq n'$, since $\theta_{\mathrm{e},m}^n$ is not a random variable anymore (60) and $\theta_{0,m}^\kappa$ is of course not independent from $\theta_{0,m}^\kappa$. In that case, $P_{\mathrm{r}}^{\mathrm{fe}}$ can be expressed as, separating the case $n = n'$ and $n \neq n'$,

$$\begin{aligned} P_{\mathrm{r}}^{\mathrm{fe}} &= P_{\mathrm{r}}^{\mathrm{fe,d}} + P_{\mathrm{r}}^{\mathrm{fe,c}}, \\ P_{\mathrm{r}}^{\mathrm{fe,d}} &= \lim_{T\to\infty} \frac{1}{2T} \int_{-T}^{T} \sum_{m,\kappa,n} E[f(m,\kappa,n)^2]dt\,, \\ P_{\mathrm{r}}^{\mathrm{fe,c}} &= \lim_{T\to\infty} \frac{1}{2T} \int_{-T}^{T} 2 \sum_{\substack{m,\kappa,n,n' \\ n>n'}} E[f(m,\kappa,n) f(m,\kappa,n')]dt, \end{aligned} \tag{55}$$

since $f(m,\kappa,n)$ and $f(m',\kappa',n')$ commutes. The power $P_{\mathrm{r}}^{\mathrm{fe,d}}$ is exactly $P_{\mathrm{r}}^{\mathrm{s}}$ (41) as provided in Section III.B. The complete derivation of $P_{\mathrm{r}}^{\mathrm{fe,c}}$ is conducted in Appendix B and final expression is given in (90). Therefore, $P_{\mathrm{r}}^{\mathrm{f}}$ is expressed as

$$\begin{aligned} P_{\mathrm{r}}^{\mathrm{fe}} &= P_{\mathrm{r}}^{\mathrm{s}} + P_{\mathrm{r}}^{\mathrm{fe,c}}, \\ P_{\mathrm{r}}^{\mathrm{fe,c}} &= \sum_{\substack{m,n,n' \\ n'>n}} \wp_m^{n,n'}\,, \end{aligned}$$

$$\begin{aligned} &\wp_m^{n,n'} \\ &= A_m^n A_m^{n'} PRF_m \left| M_{\Delta\tau_m^{n,n'}}^{\mathrm{PB}}\left(\Delta f_{D,m}^{n,n'}\right)\right| \operatorname{sinc}\left(\pi \Delta f_{D,m}^{n,n'} T_0\right) \\ &\cos\left(\pi \Delta f_{D,m}^{n,n'}(T_0 + 2\tau_m^n) - \phi\left(M_{\Delta\tau_m^{n,n'}}^{\mathrm{PB}}\left(\Delta f_{D,m}^{n,n'}\right)\right)\right. \\ &\qquad \left. + \Delta\theta_m^{n,n'}\right), \end{aligned} \tag{56}$$

where $\Delta\tau_m^{n,n'}$, $\Delta f_{D,m}^{n,n'}$ and $\Delta\theta_m^{n,n'}$ are the difference in additional delay, Doppler frequency and phase between echoes n and n' of beacon m, provided in equations (80) and (82), respectively.

The expression of $M_{\Delta\tau_m^{n,n'}}^{\mathrm{PB}}\left(\Delta f_{D,m}^{n,n'}\right)$ is given in (89) where $M_{\Delta\tau}(f)$ is the Fourier Transform (FT) of the product of two pairs of pulse delayed by $\Delta\tau$. Final expression of $M_{\Delta\tau}(f)$ is given by (without proof)

$$\begin{aligned} M_{\Delta\tau}(f) = \; & 2\sqrt{\frac{\pi}{\alpha}} e^{-\pi^2 f^2/\alpha} e^{-\alpha\frac{\Delta_\tau^2}{4}} e^{-j\pi f(\Delta\tau+\Delta t)}\,. \\ & \left(\cos(\pi f \Delta t) + e^{-\alpha\frac{\Delta t^2}{4}} ch\left(\frac{\alpha \Delta t \Delta\tau}{2}\right)\right). \end{aligned} \tag{57}$$

Finally, $\phi(M_{\Delta\tau}^{PB}(\Delta f))$ in (56) is the argument of the complex number $M_{\Delta\tau}^{\mathrm{PB}}(\Delta f)$.

C. Validation of the Average Received Power Formula Under the Fixed Environment Assumption

Formula of the post-blanker average received power (56) is validated by means of Monte-Carlo simulations.

The objective of the Monte-Carlo simulation under the fixed-environment assumption is to provide a validation vector $\aleph_{(\tau^1)}$ where each element of $\aleph$ is the ratio (in dB) of the average received power computed by the Monte-Carlo simulation, $P_{\mathrm{r}}^{\mathrm{fe,MC}}$, with the received power formula $P_{\mathrm{r}}^{\mathrm{fe}}$ provided in (56).

To derive the validation vector, a single DME beacon and one multipath ($M = 1$, $N_m = 1$) with PEP below the blanking threshold are considered. The deterministic and random parameters of the Monte-Carlo simulation for the fixed environment assumption are summarized in the second column of Table I.

The methodology to obtain the validation vector is exactly the same as the one for the validation matrix V as provided in Section III.E, the only differences being that only one MP is considered but 54 composite pulses are received within $T_0 = 20$ ms. Therefore, 54 values of t^{κ} and θ_0^{κ} are drawn for each Monte-Carlo simulations.

Fig. 8 provides (a) the validation vector $\aleph_{(\tau^1)}$ and (b) the outputs of $P_{\mathrm{r}}^{\mathrm{fe}}$ (in dashed orange) and $P_{\mathrm{r,MC}}^{\mathrm{fe}}$ (in blue) for each of the possible value of τ^1, in W.

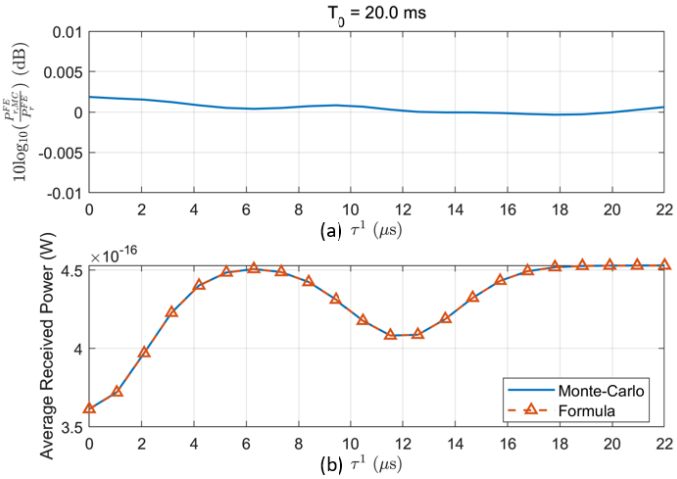

Fig. 8. (a) Results of the validation vector $\aleph_{(\tau^1)}$ for the Monte-Carlo simulations under the fixed environment assumption and (b) outputs of $P_{\mathrm{r}}^{\mathrm{fe}}$ (in dashed orange) and $P_{\mathrm{r,MC}}^{\mathrm{fe}}$ (in blue) for each of the possible value of τ^1.

Fig. 8 (a) shows that the ratio between $P_{\mathrm{r,MC}}^{\mathrm{fe}}$ and $P_{\mathrm{r}}^{\mathrm{fe}}$ (56) never exceeds 0.005 dB and thus (56) is validated.

D. Average Received Power Discussion and Impact on $\mathrm{PW}_m^{\mathrm{eq,n}}$ and $\mathrm{pw}_m^{\mathrm{eq,n}}$

The average received power under the fixed environment assumption $P_{\mathrm{r}}^{\mathrm{fe}}$ may differ from the average received power under the statistical assumption if the cross-terms $P_{\mathrm{r}}^{\mathrm{fe,c}}$ in $P_{\mathrm{r}}^{\mathrm{fe}}$ are not zero (or negligible with respect to $P_{\mathrm{r}}^{\mathrm{s}}$) (56). If $P_{\mathrm{r}}^{\mathrm{fe,c}}$ is negligible, individual Gaussian pulses can not be processed independently: their original gaussian shape is modified and thus the true sum of the pulses instantaneous power envelope must be performed before doing any derivation.

In particular, if $P_{\mathrm{r}}^{\mathrm{fe,c}}$ is not negligible, the expression of $I_{\mathrm{bdc},m}$ as defined under the statistical assumption in (38) could be modified since the blanked interval generated by a received composite pulse can no longer be the union of the blanked interval generated by all the received pulses: they first must be summed together and after $I_{\mathrm{bdc},m}$ can be derived. In that case, no analytical formula can be found for $I_{\mathrm{bdc},m}$ and thus $I_{\mathrm{bdc},m}$ can only be numerically obtained by comparing the instantaneous power envelope of the sum to the blanking threshold.

Therefore, under the fixed environment assumption, no closed form can be found for $\mathrm{pw}_m^{\mathrm{eq}}$ as defined in (12) if $P_{\mathrm{r}}^{\mathrm{fe,c}}$ is not negligible.

Furthermore, under the fixed environment assumption, the mathematical expression of $\mathrm{PW}_m^{\mathrm{eq}}$ is retrieved from (18) and from the expression of the average post blanker received power (56) as

$$\begin{aligned} P_{\mathrm{r}}^{\mathrm{fe}} &= \sum_{m=1}^{M} \left(P_{\mathrm{r},m}^{\mathrm{s}} + P_{\mathrm{r},m}^{\mathrm{fe,c}}\right), \\ P_{\mathrm{r},m}^{\mathrm{s}} + P_{\mathrm{r},m}^{\mathrm{fe,c}} &= \mathrm{PEP}_m^0 \mathrm{PW}_m^{eq} \mathrm{PRF}_m, \\ \mathrm{PW}_m^{eq} &= \sum_{n} \frac{\mathrm{PEP}_m^n}{\mathrm{PEP}_m^0} \mathrm{PW}_m^{\mathrm{eq},n} + \sum_{\substack{n,n' \\ n'>n}} \frac{\wp_m^{n,n'}}{\mathrm{PEP}_m^0 \mathrm{PRF}_m} \end{aligned} \tag{58}$$

In (59), even if the analytical formula for $\wp_m^{n,n'}$ is known and expressed in (56), $\mathrm{PW}_m^{\mathrm{eq},n}$ as expressed in (43) does not have a closed form if $P_{\mathrm{r}}^{\mathrm{fe,c}}$: it can still be expressed by means of erfc but the bounds of the disjoint intervals $\mathrm{l}_{\mathrm{d},m}^q$ and $\mathrm{r}_{\mathrm{d},m}^q$ can only be obtained numerically.

E. Definition of Applicability Zone

Since no closed forms of PW_m^{eq} and $\mathrm{pw}_m^{\mathrm{eq}}$ are found under the fixed environment in case $P_{\mathrm{r}}^{\mathrm{fe,c}}$ is not negligible with respect to $P_{\mathrm{r}}^{\mathrm{s}}$, it is natural to define applicability zones where $P_{\mathrm{r}}^{\mathrm{fe,c}}$ may be neglected. In this article, a zone is said "applicable" if the closed form formulas $\mathrm{pw}_m^{\mathrm{eq}}$ (40) and PW_m^{eq} (49) of the statistical model can be used even under the fixed environment assumption.

Therefore, three zones of applicability are defined in this section.

Zone 1: In the first zone, $P_{\mathrm{r}}^{\mathrm{fe,c}}$ is negligible with respect to $P_{\mathrm{r}}^{\mathrm{s}}$ and therefore the gaussian shape of the pulse is not modified in term of envelope. In that case, $\mathrm{pw}_m^{\mathrm{eq}}$ (40) and PW_m^{eq} (49) of the statistical model can still be used under the environment fixed assumption.

Zone 2: In the second zone, $P_{\mathrm{r}}^{\mathrm{fe,c}}$ is not directly negligible with respect to $P_{\mathrm{r}}^{\mathrm{s}}$ but $P_{\mathrm{r}}^{\mathrm{fe,c}}$ can be combined with $P_{\mathrm{r}}^{\mathrm{s}}$ such that the resulting envelope of the gaussian pulses is a gaussian pulse whose amplitude is the sum of the amplitudes of the gaussian pulses. Therefore, $\mathrm{pw}_m^{\mathrm{eq}}$ (40) and PW_m^{eq} (49) can still be used in that zone.

Zone 3: The third zone is defined as the zone where $P_{\mathrm{r}}^{\mathrm{fe,c}}$ is neither negligible with respect to $P_{\mathrm{r}}^{\mathrm{s}}$ nor can be combined with $P_{\mathrm{r}}^{\mathrm{s}}$. In that case, $\mathrm{pw}_m^{\mathrm{eq}}$ (40) and PW_m^{eq} (49) can not be used and no closed form are available for $\mathrm{pw}_m^{\mathrm{eq}}$ and PW_m^{eq} under the fixed environment assumption.

To simplify the mathematical definition of the three zones, the notation of $P_{\mathrm{r,m}}^{\mathrm{s}}$ from (41) is updated into

$$\begin{aligned} P_{\mathrm{r,n}}^{\mathrm{s}} &= \sum_n u_m^n\,, \\ u_m^n &= \mathrm{PEP}_m^n \mathrm{PW}_m^{\mathrm{eq},n} \mathrm{PRF}_m \text{ and} \\ u_m^{n_0 \oplus n} &= \frac{\left(A_m^{n_0} + A_m^n\right)^2}{2} \mathrm{PW}_m^{\mathrm{eq},n \oplus n'} \mathrm{PRF}_m, \end{aligned} \tag{60}$$

where $\mathrm{PW}_m^{\mathrm{eq},n\oplus n'}$ is the equivalent pulse width of the gaussian pulse whose complex amplitude is the sum of the complex of pulse n and n'.

Zones are always defined by fixing a reference scatterer n_0 in the set of the N_m scatterers in the RLOS of beacon m. Once the reference scatterer is set, zones are determined by investigating the average received power as if only two echoes (n_0, n) were received, where n goes through $[\![1, N_m - 1]\!]$ since $n \neq n_0$.

The average received power under the fixed environment assumptions $P_{\mathrm{r}}^{\mathrm{fe}}$ when two echoes (n_0, n) are received using (60) notations is simply expressed as

$$P_{\mathrm{r}}^{\mathrm{fe}} = P_{\mathrm{r}}^{\mathrm{s}} + P_{\mathrm{r}}^{\mathrm{fe,c}} = u_m^{n_0} + u_m^n + \wp_m^{n_0,n} \tag{61}$$

Using these notations, the three zones are mathematically defined below. The first zone $Z_{1,m}^{n_0}$ is defined as the set of echoes n whose cross term $\wp_m^{n_0,n}$ is considered to be negligible compared to the direct term $u_m^{n_0} + u_m^n$. Therefore, zone $Z_{1,m}^{n_0}$ is mathematically defined as

$$Z_{1,m}^{n_0} \coloneqq \left\{ n \in [\![0, N_m - 1]\!] \,\middle|\, \left| \frac{\wp_m^{n_0,n}}{u_m^{n_0} + u_m^n} \right| < \epsilon_1 \right\} \tag{62}$$

where ϵ_1 is defined to be either 0.01 or 0.05 in this work.

Second zone $Z_{2,m}^{n_0}$ corresponds to the set of echoes n that are not in $Z_{1,m}^{n_0}$ and whose cross term is not negligible but combine with the direct term such that PW_m^{eq} and $\mathrm{pw}_m^{\mathrm{eq}}$ from the statistical model are applicable to the single echo $n_0 \oplus n$ whose amplitude is the sum of the amplitudes of echoes (n_0, n). Therefore, $Z_{2,m}^{n_0}$ is mathematically defined as

$$Z_{2,m}^{n_0} \coloneqq \left\{ n \in [\![0, N_m - 1]\!] \,\middle|\, \left| \frac{u_m^{n_0 \oplus n}}{u_m^{n_0} + u_m^n + \wp_m^{n_0,n}} \right| > 1 - \epsilon_2 \right\} \bigcap \overline{Z_{1,m}^{n_0}} \tag{63}$$

where ϵ_2 is defined to be either 0.01 or 0.05 in this work.

Finally, third zone is defined as the set of echoes n that are neither in $Z_{1,m}^{n_0}$ nor in $Z_{2,m}^{n_0}$ and whose cross term $\wp_m^{n_0,n}$ with respect to n_0 is not negligible compared to the direct term. Therefore, $Z_{3,m}^{n_0}$ is mathematically defined as

$$Z_{3,m}^{n_0} \coloneqq \left\{ n \in [\![0, N_m - 1]\!] \,\middle|\, \left| \frac{\wp_m^{n_0,n}}{u_m^{n_0} + u_m^n} \right| < 1 - \epsilon_1 \right\} \bigcap \overline{\left(Z_{1,m}^{n_0} \bigcup Z_{2,m}^{n_0} \right)} \tag{64}$$

F. Illustration of Applicability Zones

The objective of the presented illustrations is to provides a graphical example of applicability zones for a simple scene. The scene is composed of a single DME beacon and an aircraft separated by a slant range of 50 km. The aircraft is supposed to be in approach phase, at 2100 feet above ground, its velocity is set to 115 knots and its glide angle to 5° [13]. The direction in the azimuthal plane of the aircraft speed vector is set to North and East. The RLOS of the beacon is defined to be a circle around the beacon with radius of 25 km as defined in [8]. Since only one beacon is considered, the subindex m is discarded.

Zones are function of $\wp^{n_0,n}$, u^{n_0}, u^n and $u^{n_0\oplus n}$ defined in (60) and (56) and therefore all the parameters involved in their equations must either be inputs or determined by the inputs of the illustration.

For the purpose of the illustration, all the parameters except for $\Delta\tau^{n_0,n}$ and $\Delta f_{\mathrm{D}}^{n_0,n}$ are fixed as inputs. The carrier frequency f of the beacon is set to 1176 MHz. The PEP of any scatterers within the RLOS is set to -122 dBW and therefore the blanker is never triggered. PRF is set to 2700. The difference in additional phase $\Delta\theta^{n_0,n}$ is set to 45°. Note that the influence of $\Delta\theta^{n_0,n}$ was found to have a small impact on the final results and therefore only one value is chosen for this illustration.

The value of T_0 may be discussed. A small T_0 implies a greater invalidity zone, i.e., zone 3 because the potential full swept of the phase difference (statistical assumption) is unlikely to happen during that time. Therefore, zone 3 is expected to shrink and zone 1 is expected to grow as T_0 increases. Consequently, two values of T_0, 20 ms and 1 s, are investigated. Finally, two values for ϵ_1 and ϵ_2, 0.01 and 0.05, are set. The illustrations associated with $\epsilon_1 = \epsilon_2 = 0.01$ and $\epsilon_1 = \epsilon_2 = 0.05$ are referred as illustration 1 and illustration 2, respectively.

Once the inputs are set, the methodology to obtain the positions of the scatterers within the different zones is as follows:

1. Determination of the zone matrix $(\mathrm{W})_{(\Delta\tau,\Delta f_D)}$ for generic values of $\Delta\tau$ and Δf_D.
2. Choice of the position of the reference scatterers.
3. Covering of the RLOS where $\Delta\tau^{n_0,n}$ and $\Delta f_{\mathrm{D}}^{n_0,n}$ are derived with respect to each reference scatterers and plotting of the different zones.

The three steps are detailed below.

Determination of the zone matrix $(W)_{(\Delta\tau,\Delta f_D)}$*:* The zone matrix $(\mathrm{W})_{(\Delta\tau,\Delta f_D)}$ is determined for generic values of $\Delta\tau$ and Δf_D in a conservative range of $[-200,200]$ µs and $[-200,200]$ Hz, respectively. Each element of W is associated to one value of $\Delta\tau$ and Δf_D within their respected range. With the value of $\Delta\tau$ and Δf_D, the value of $\wp^{n_0,n}$, u^{n_0}, u^n and $u^{n_0\oplus n}$ are determined and the corresponding zone (1,2 or 3) is saved inside W.

Choice of the position of the reference scatterers: Four different reference scatterers are chosen for this illustration. Their positions is chosen in the four quadrants on the RLOS of the DME/TACAN beacon.

Covering of the RLOS: For each reference scatterers, the RLOS is covered and for each point within the RLOS, one value of $\Delta\tau^{n_0,n}$ and $\Delta f_{\mathrm{D}}^{n_0,n}$ is determined. The zone of the pair $\left(\Delta\tau^{n_0,n},\Delta f_{\mathrm{D}}^{n_0,n}\right)$ is then simply retrieved by looking into the zone matrix W at the corresponding indices.

Fig. 9 and Fig. 10 provides the illustration for $\epsilon_1=\epsilon_2=0.01$ and $\epsilon_1=\epsilon_2=0.05$ respectively. For each illustration, the aircraft velocity azimuth angle is directed either to (a) North or to (b) East. Zones are represented by a color. For $T_0=20$ ms, Zones 1, 2 and 3 are displayed in white, blue and red, respectively. For $T_0=1$ s, Zones 1, 2 and 3 are displayed in white, cyan and orange, respectively. The 4 reference scatterers are represented by black squares.

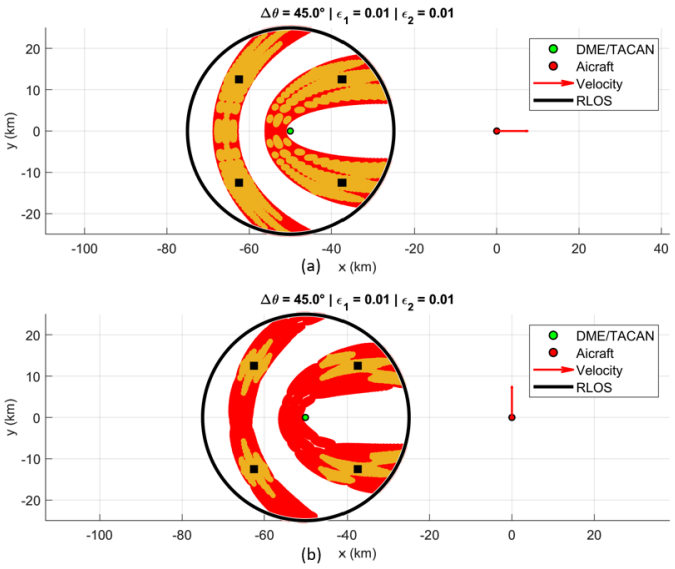

Fig. 10. Graphical illustration of the applicability zones for $\epsilon_1=\epsilon_2=0.01$, $T_0=20$ ms or 1 s and aircraft velocity (a) North and (b) East.

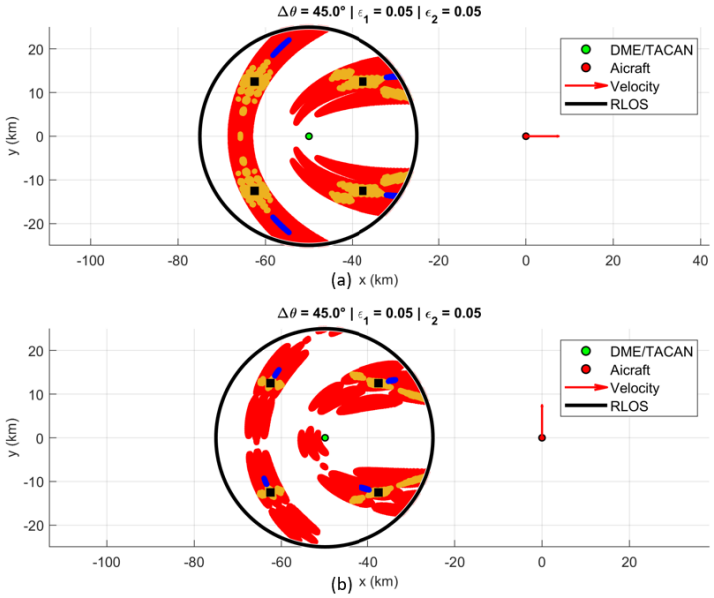

Fig. 9. Graphical illustration of the applicability zones for $\epsilon_1=\epsilon_2=0.05$, $T_0=20$ ms or 1 s and aircraft velocity (a) North and (b) East.

Three concluding remarks can be made regarding Fig. 9 and Fig. 10:

1. Zone 2 associated with $T_0=1$ s (cyan) is nowhere to be seen in both figures. It is because only scatterers extremely close to the reference scatterers can be combined to create the gaussian pulse whose amplitude is the sum of both amplitudes and thus zone 2 is too small to be seen in the plot.
2. The more the thresholds $\epsilon_1=\epsilon_2$ increase, the smaller non applicability zone 3 is. This is because it is less difficult to be in Zone 1, i.e., cross terms from $P_{\mathrm{r}}^{\mathrm{fe,c}}$ need less to be negligible with respect to $P_{\mathrm{r}}^{\mathrm{s}}$.
3. The more T_0 increases, the smaller zone 2 and zone 3 are. This is because the potential full swept of the phase difference, i.e., statistical assumption, is more likely to happen when T_0 increases and therefore the smaller are zone 2 and zone 3, as expected.

V. CONCLUSION

In this article, the MP-free C/N_0 degradation model developed in [1] has been updated to include MP generated by ground scatterers located in the RLOS of the DME/TACAN beacons. The MP-free C/N_0 degradation model relies on the definition of $\mathrm{pw}^{\mathrm{eq}}$ and $\mathrm{PW}^{\mathrm{eq}}$ that have been updated and customized in presence of MP for two different set of assumptions: the statistical and the fixed environment assumptions.

Under the statistical assumption, it has been shown that the received pulses contributions may be investigated independently, i.e., by preserving their original Gaussian shapes. In that case, $\mathrm{pw}^{\mathrm{eq}}$ and $\mathrm{PW}^{\mathrm{eq}}$ have been updated and

closed-form formulas were found, by means of erfc functions. The necessary inputs to apply the statistical model have been highlighted since Part II of this work intends to use the statistical model at two low-altitude operation hot-spots: JALTO (Philadelphia) and TIXAK (Frankfort) [8].

Under the fixed environment assumption, $\mathrm{pw}^{\mathrm{eq}}$ and $\mathrm{PW}^{\mathrm{eq}}$ have been updated but closed-form formulas may not be found since received pulses may not be investigated independently. Therefore, an additional study has been provided to mathematically define applicability zones where closed-form formulas, that are the same as the statistical ones, may be used. Finally, a graphical illustration of the applicability zones has been provided for a simple DME/TACAN beacon/aircraft configuration for different values of T_0, ϵ_1 and ϵ_2.

APPENDIX A
Average Power Derivation – Statistical Assumption

In this appendix, the derivation of the average power of $r(t)$ (27) under the statistical assumption (29) is conducted. In the statistic case, the average power $P_{\mathrm{r}}^{\mathrm{s}}$ from (34) is given by

$$P_{\mathrm{r}}^{s} = \lim_{T\to\infty} \frac{1}{2T} \int_{-T}^{T} \sum_{m,\kappa,n} E[f(m,\kappa,n)^2]dt\,. \tag{65}$$

where

$$\begin{aligned} E[f(m,\kappa,n)^2] = (A_m^n)^2 E[g(t-t_m^\kappa-\tau_m^n)^2 \cdot \\ b_m(t-t_m^\kappa-\tau_m^0)^2 \cos\big(2\pi\big(f_m+f_{D,m}^n\big)t \\ +\theta_m^{\kappa,n}\big)^2]. \end{aligned} \tag{66}$$

Furthermore, $b_m(t-t_m^\kappa-\tau_m^0)^2 = b_m(t-t_m^\kappa-\tau_m^0)$, $t_m^\kappa \perp \theta_m^{\kappa,n}$ and $\cos^2(x) = \frac{1-\cos(2x)}{2}$. Therefore,

$$\begin{aligned} E[f(m,\kappa,n)^2] = \frac{(A_m^n)^2}{2} E[g(t-t_m^\kappa-\tau_m^n)^2 b_m(t \\ -t_m^\kappa-\tau_m^0)], \end{aligned} \tag{67}$$

since, by the law of total expectation,

$$E\big[\cos\big(4\pi\big(f_m+f_{D,m}^n\big)t+2\theta_m^{\kappa,n}\big)\big] = 0. \tag{68}$$

Furthermore, since $t_m^\kappa \sim U[0,T_0]$

$$\begin{aligned} P_{\mathrm{r}}^{s} = \lim_{T\to\infty} \frac{1}{2T} \int_{-T}^{T} \sum_{m,\kappa,n} \frac{(A_m^n)^2}{2T_0} \int_0^{T_0} g(t-t_m^\kappa \\ -\tau_m^n)^2 b_m(t-t_m^\kappa-\tau_m^0) dt_m^\kappa\, dt\,. \end{aligned} \tag{69}$$

Assume $\mathrm{K}_m(T)$ to be the number of received pulse pairs during $[-T,T]$, then, interchanging sums (where now $\kappa \in [\![1, \mathrm{K}_m(t)]\!]$) and integral and using Fubini's theorem,

$$\begin{aligned} P_{\mathrm{r}}^{s} &= \lim_{T\to\infty} \frac{1}{2T} \sum_{m,\kappa,n} \frac{\mathrm{PEP}_m^n}{T_0} \int_0^{T_0} I(t_m^\kappa)\, dt_m^\kappa \\ I(t_m^\kappa) &= \int_{-T}^{T} h(t)dt \\ h(t) &= g(t-t_m^\kappa-\tau_m^n)^2 b_m(t-t_m^\kappa-\tau_m^0) \end{aligned} \tag{70}$$

Therefore, there is no terms inside the sum which depends on κ. This yields,

$$\begin{aligned} P_{\mathrm{r}}^{s} &= \lim_{T\to\infty} \frac{1}{2T} \sum_{m,n} \frac{K_m(T)\mathrm{PEP}_m^n}{T_0} \int_0^{T_0} I(t_m^\kappa)\, dt_m^\kappa \\ P_{\mathrm{r}}^{s} &= \sum_{m,n} \lim_{T\to\infty} \left(P_{\mathrm{r}}^{s,1}(T) \cdot P_{\mathrm{r}}^{s,2}(T)\right), \end{aligned} \tag{71}$$

where

$$\begin{aligned} P_{\mathrm{r}}^{s,1}(T) &= \frac{K_m(T)}{2T}, \\ P_{\mathrm{r}}^{s,2}(T) &= \frac{\mathrm{PEP}_m^n}{T_0} \int_0^{T_0} I(t_m^\kappa)\, dt_m^\kappa. \end{aligned} \tag{72}$$

Assuming that both limits of $P_{\mathrm{r}}^{s,1}(T)$ and $P_{\mathrm{r}}^{s,2}(T)$ are finites (which will be shown later in the derivation), the limit can be linearized into

$$P_{\mathrm{r}}^{s} = \sum_{m,n} \lim_{T\to\infty} \left(P_{\mathrm{r}}^{s,1}(T)\right) \cdot \lim_{T\to\infty} \left(P_{\mathrm{r}}^{s,2}(T)\right), \tag{73}$$

where

$$\begin{aligned} \lim_{T\to\infty} \left(P_{\mathrm{r}}^{s,1}(T)\right) &= \lim_{T\to\infty} \left(\frac{K_m(T)}{2T}\right) \\ &= \mathrm{PRF}_{\mathrm{m}} \end{aligned} \tag{74}$$

as PRF is defined as an average pulse repetition frequency and

$$\begin{aligned} \lim_{T\to\infty} \left(P_{\mathrm{r}}^{s,2}(T)\right) &= \lim_{T\to\infty} \left(\frac{\mathrm{PEP}_m^n}{T_0} \int_0^{T_0} I(t_m^\kappa)\, dt_m^\kappa \right) \\ &= \frac{\mathrm{PEP}_m^n}{T_0} \int_0^{T_0} \lim_{T\to\infty} \int_{-T}^{T} h(t)dtdt_m^\kappa \\ &= \frac{\mathrm{PEP}_m^n}{T_0} \int_0^{T_0} \int_{-\infty}^{\infty} h(t)dtdt_m^\kappa. \end{aligned} \tag{75}$$

Furthermore,

$$\int_{-\infty}^{\infty} h(t)dt = \int_{-\infty}^{\infty} g(t - t_m^{\kappa} - \tau_m^n)^2 b_m(t - t_m^{\kappa} - \tau_m^0)dt = \int_{-\infty}^{\infty} e^{-\alpha(u-\tau_m^n)^2} b_m(u - \tau_m^0)du \tag{76}$$

which does not depend on κ. Therefore, from (73), the final expression of $P_{\mathrm{r}}^{\mathrm{s}}$ is given by

$$P_{\mathrm{r}}^{\mathrm{s}} = \sum_{m,n} \frac{\mathrm{PRF_m PEP}_m^n}{T_0} \int_0^{T_0} \int_{-\infty}^{\infty} h(t)dt\, dt_m^{\kappa} = \sum_{m,n} \mathrm{PRF_m PEP}_m^n \int_{-\infty}^{\infty} e^{-\alpha(u-\tau_m^n)^2} b_m(u - \tau_m^0)du\,. \tag{77}$$

APPENDIX B
Average Power Derivation – Fixed Environment Assumption

In this appendix, the derivation of the average power of $r(t)$ (53) under the fixed environment assumption (54) is conducted. In the fixed environment case, the average received power $P_{\mathrm{r}}^{\mathrm{fe}}$ (55) is given by

$$P_{\mathrm{r}}^{\mathrm{fe}} = P_{\mathrm{r}}^{\mathrm{s}} + P_{\mathrm{r}}^{\mathrm{fe,c}},$$
$$P_{\mathrm{r}}^{\mathrm{fe,c}} = \lim_{T\to\infty} \frac{1}{2T} \int_{-T}^{T} 2 \sum_{\substack{m,\kappa,n,n' \\ n>n'}} E[f(m,\kappa,n) f(m,\kappa,n')]dt, \tag{78}$$

where $P_{\mathrm{r}}^{\mathrm{s}}$ is provided in (77). Let $E_f^{n,n'}$ be $E[f(m,\kappa,n)f(m,\kappa,n')]$ then, since $t_m^{\kappa} \perp \theta_m^{\kappa,n}$,

$$E_f^{n,n'} = \frac{A_m^n A_m^{n'}}{2} \cdot E\left[m_{\Delta\tau_m^{n,n'}}(t - t_m^{\kappa} - \tau_m^n) b_m(t - t_m^{\kappa} - \tau_m^0)^2\right] \cdot E[\cos\left(\left(2\pi(f_m + f_{D,m}^n)t + \theta_m^{\kappa,n}\right)\right) \cdot \cos\left(\left(2\pi(f_m + f_{D,m}^{n'})t + \theta_m^{\kappa,n'}\right)\right)], \tag{79}$$

where $m_{\Delta\tau}(t)$ is the product of two pulse pairs delayed by $\Delta\tau$ and $\Delta\tau_m^{n,n'}$ is the additional delay difference between echo n and n' and, i.e.,

$$\begin{aligned} m_{\Delta\tau}(t) &= s_{bb}(t) s_{bb}(t - \Delta\tau) \\ \Delta\tau_m^{n,n'} &= \tau_m^{n'} - \tau_m^n. \end{aligned} \tag{80}$$

Furthermore, since $b_m(t - t_m^{\kappa} - \tau_m^0)^2 = b_m(t - t_m^{\kappa} - \tau_m^0)$, $\theta_m^{\kappa,n} \sim U[0,2\pi)$ and using trigonometry formula for $\cos(a)\cos(b)$,

$$E_f^{n,n'} = \frac{A_m^n A_m^{n'}}{2} E\left[m_{\Delta\tau_m^{n,n'}}(t - t_m^{\kappa} - \tau_m^n) b_m(t - t_m^{\kappa} - \tau_m^0)\right] \cdot \cos\left(2\pi\left(\Delta f_{D,m}^{n,n'}\right)t + \Delta\theta_m^{n,n'}\right), \tag{81}$$

where $\Delta f_{D,m}^{n,n'}$ and $\Delta\theta_m^{n,n'}$ are the difference Doppler frequency and phase between echoes n and n' of beacon m, i.e.,

$$\begin{aligned} \Delta f_{D,m}^{n,n'} &= f_{D,m}^{n'} - f_{D,m}^n \\ \Delta\theta_m^{n,n'} &= \theta_m^{\kappa,n'} - \theta_m^{\kappa,n}. \\ &= \left(\theta_{\mathrm{D},m}^{n'} + \theta_{\mathrm{e},m}^{n'}\right) - \left(\theta_{\mathrm{D},m}^{n} + \theta_{\mathrm{e},m}^{n}\right) \end{aligned} \tag{82}$$

Assume that the number of pulse pairs emitted during $[-T,T]$ is $\mathrm{K}_m(T)$ then, interchanging sums (where now $\kappa \in [\![1, \mathrm{K}_m(t)]\!]$) and integral

$$P_{\mathrm{r}}^{\mathrm{fe,c}} = \lim_{T\to\infty} \frac{1}{T} \sum_{\substack{m,\kappa,n,n' \\ n>n'}} \frac{A_m^n A_m^{n'}}{2} \cdot \int_{-T}^{T} E\left[m_{\Delta\tau_m^{n,n'}}(t - t_m^{\kappa} - \tau_m^n) b_m(t - t_m^{\kappa} - \tau_m^0)\right] \cdot \cos\left(2\pi\left(\Delta f_{D,m}^{n,n'}\right)t + \Delta\theta_m^{n,n'}\right) dt \tag{83}$$

Since $t_m^{\kappa} \sim U[0,T_0]$ and using Fubini's theorem,

$$\begin{aligned} P_{\mathrm{r}}^{\mathrm{fe,c}} &= \lim_{T\to\infty} \frac{1}{T} \sum_{\substack{m,\kappa,n,n' \\ n>n'}} \frac{A_m^n A_m^{n'}}{2T_0} \int_0^{T_0} J(t_m^{\kappa})dt_m^{\kappa}, \\ J(t_m^{\kappa}) &= \int_{-T}^{T} a(t)\cos\left(2\pi\left(\Delta f_{D,m}^{n,n'}\right)t + \Delta\theta_m^{n,n'}\right) dt \\ a(t) &= b_m(t - t_m^{\kappa} - \tau_m^0) m_{\Delta\tau_m^{n,n'}}(t - t_m^{\kappa} - \tau_m^n). \end{aligned} \tag{84}$$

Therefore, there is no term inside the sum which depends on κ. This yields,

$$\begin{aligned} P_{\mathrm{r}}^{\mathrm{fe,c}} &= \sum_{\substack{m,n,n' \\ n'>n}} \lim_{T\to\infty} \left(P_{\mathrm{r}}^{\mathrm{fe,c,1}}(T) \cdot P_{\mathrm{r}}^{\mathrm{fe,c,2}}(T)\right), \\ P_{\mathrm{r}}^{\mathrm{fe,c,1}}(T) &= \frac{K_m(T)}{2T}, \\ P_{\mathrm{r}}^{\mathrm{fe,c,2}}(T) &= \frac{A_m^n A_m^{n'}}{T_0} \int_0^{T_0} J(t_m^{\kappa})\, dt_m^{\kappa}. \end{aligned} \tag{85}$$

Assuming that both limits of $P_{\mathrm{r}}^{\mathrm{f,c,1}}(T)$ and $P_{\mathrm{r}}^{\mathrm{f,c,1}}(T)$ are finites (which will be shown later in the derivation), the limit can be linearized into, as explained in Appendix A,

$$\begin{aligned} P_{\mathrm{r}}^{\mathrm{fe,c}} &= \sum_{\substack{m,n,n' \\ n'>n}} \lim_{T\to\infty}\left(P_{\mathrm{r}}^{\mathrm{fe,c,1}}(T)\right)\cdot\lim_{T\to\infty}\left(P_{\mathrm{r}}^{\mathrm{fe,c,1}}(T)\right), \\ &= \sum_{\substack{m,n,n' \\ n'>n}} \mathrm{PRF_m}\cdot\frac{A_m^n A_m^{n'}}{T_0}\int_0^{T_0}\int_{-\infty}^{\infty} a(t)\cdot \\ &\quad \cos\left(2\pi\left(\Delta f_{D,m}^{n,n'}\right)t+\Delta\theta_m^{n,n'}\right)dt_m^{\kappa} \end{aligned} \tag{86}$$

Furthermore, using Parseval's identity and the Hermitian property of the Fourier transform (FT) of a real signal,

$$\begin{aligned} &\int_{-\infty}^{+\infty} a(t)\cdot\cos(2\pi f_0 t+\theta)\,dt \\ &\qquad = |A(f_0)|\cos\left(\theta-\phi(f_0)\right), \end{aligned} \tag{87}$$

Where $A(f)$ is the FT of $a(t)$ and the function ϕ is the argument of $A(f)$. Therefore, using the definition of $a(t)$ (84) and the change of variable $u = t - t_m^{\kappa} - \tau_m^n$, f_0 from (87) is identified as $\Delta f_{D,m}^{n,n'}$ and θ as $2\pi\Delta f_{D,m}^{n,n'}(t_m^{\kappa}+\tau_m^n)+\Delta\theta_m^{n,n'}$. This yields

$$\begin{aligned} P_{\mathrm{r}}^{\mathrm{fe,c}} = \sum_{\substack{m,n,n' \\ n'>n}} \mathrm{PRF_m}\cdot\frac{A_m^n A_m^{n'}}{T_0}\int_0^{T_0}\left|M^{PB}_{\Delta\tau_{\mathrm{m}}^{\mathrm{n,n'}}}\left(\Delta f_{D,m}^{n,n'}\right)\right|\cdot \\ \cos\left(\begin{matrix}2\pi\Delta f_{D,m}^{n,n'}(t_m^{\kappa}+\tau_m^n)+\Delta\theta_m^{n,n'}- \\ \phi\left(M^{\mathrm{PB}}_{\Delta\tau_m^{n,n'}}\left(\Delta f_{D,m}^{n,n'}\right)\right)\end{matrix}\right)dt_m^{\kappa}, \end{aligned} \tag{88}$$

where

$$\begin{aligned} M^{PB}_{\Delta\tau_{\mathrm{m}}^{\mathrm{n,n'}}}\left(\Delta f_{D,m}^{n,n'}\right) &= M_{\Delta\tau_{\mathrm{m}}^{\mathrm{n,n'}}}\left(\Delta f_{D,m}^{n,n'}\right) \\ &\quad * \mathrm{FT}\left(b_m(u+\tau_m^n-\tau_m^0)\right)\Big|_{\Delta f_{D,m}^{n,n'}} \end{aligned} \tag{89}$$

Finally, $M^{PB}_{\Delta\tau_{\mathrm{m}}^{\mathrm{n,n'}}}\left(\Delta f_{D,m}^{n,n'}\right)$ does not depend on t_m^{κ} and therefore the integral in (88) has a well-known closed form from typical GNSS correlator output derivation such that [14]

$$\begin{aligned} P_{\mathrm{r}}^{\mathrm{f,c}} = \sum_{\substack{m,n,n' \\ n'>n}} \mathrm{PRF_m}A_m^n A_m^{n'}\left|M^{\mathrm{PB}}_{\Delta\tau_{\mathrm{m}}^{\mathrm{n,n'}}}\left(\Delta f_{D,m}^{n,n'}\right)\right|\cdot \\ \mathrm{sinc}\left(\pi\Delta f_{D,m}^{n,n'}T_0\right)\cos(\pi\Delta f_{D,m}^{n,n'}(T_0+2\tau_m^n)+ \\ \Delta\theta_m^{n,n'}-\phi\left(M^{\mathrm{PB}}_{\Delta\tau_m^{n,n'}}\left(\Delta f_{D,m}^{n,n'}\right)\right)) \end{aligned} \tag{90}$$

which concludes the derivation of $P_{\mathrm{r}}^{\mathrm{f,c}}$.

REFERENCES

[1] RTCA, "DO 292 - Assessment of Radio Frequency Interference Relevant to the GNSS L5/E5A Frequency Band," Jul. 2004. [Online]. Available: https://bovin.recherche.enac.fr/owncloud/index.php/apps/files/ajax/download.php?dir=%2FDocuments%2FR%C3%A9f%C3%A9rences%2FRTCA%2BICAO%20documents%2F&files=RTCA%20-%202004%20-%20DO%20292%20-%20Assessment%20of%20Radio%20Frequency%20Interference%20Relevant%20to%20the%20GNSS%20L5E5A%20Frequency%20Band.pdf

[2] F. Bastide, "Analysis of the Feasibility and Interests of Galileo E5a/E5b and GPS L5 for Use with Civil Aviation," Institut National Polytechnique de Toulouse, France, 2004.

[3] C. Hegarty, T. Kim, S. Ericson, P. Reddan, T. Morrissey, and A. J. Van Dierendonck, "Methodology for Determining Compatibility of GPS L5 with Existing Systems and Preliminary Results," presented at the Proceedings of The Institute of Navigation Annual Meeting, Cambridge, MA, Jun. 1999.

[4] C. Hegarty, A. J. Van Dierendonck, D. Bobyn, M. Tran, T. Kim, and J. Grabowski, "Suppression of Pulsed Interference through Blanking," presented at the Proceedings of the Institute of Navigation Annual Meeting, Fairvax, VA, Jun. 2000.

[5] A. Garcia-Pena, O. Julien, P. V. Gakne, C. Macabiau, M. Mabilleau, and P. Durel, "Efficient DME/TACAN Blanking Method for GNSS-based Navigation in Civil Aviation," presented at the ION GNSS+ 2019, 32nd International Technical Meeting of the Satellite Division of The Institute of Navigation, Miami, Florida, Sep. 2019. [Online]. Available: https://hal-enac.archives-ouvertes.fr/hal-03001697

[6] A. Garcia-Pena, C. Macabiau, M. Mabilleau, and P. Durel, "Impact of DME/TACAN on GNSS L5/E5a Receiver," presented at the ITM 2020, International Technical Meeting, San Diego, California, Jan. 2020.

[7] A. Garcia-Pena, O. Julien, C. Macabiau, M. Mabilleau, and P. Durel, "GNSS C/N0 degradation model in presence of continuous wave and pulsed interference," NAVIGATION.2021;68:75–91. [Online]. Available: https://doi.org/10.1002/navi.405

[8] N. Gault, A. Chabory, A. Garcia-Pena, and C. Macabiau, “DME/TACAN multipath Impact on GNSS L5/E5a Airborne Receivers Part II: Air-To-Ground Channel Model and Application,” *IEEE Trans. Aerosp. Electron. Syst.*
[9] N. Gault, A. Garcia-Pena, A. Chabory, and C. Macabiau, “Impact of DME/TACAN on GNSS L5/E5a Receiver at Low Altitude Considering Multipath,” presented at the Proceedings of the 35th International Technical Meeting of the Satellite Division of the Institute of Navigation (ION GNSS+ 2022), Denver, Sep. 2022.
[10] R. C. Borden, C. C. Trout, and E. C. Williams, “Description and evaluation of 100-channel Distance-Measuring Equipment,” presented at the Proceedings of the IRE, vol. 39, no. 6, pp. 612-618, doi: 10.1109/JRPROC.1951.233461., Jun. 1951.
[11] L. Kleinrock, *Queing Systems*, vol. 1. New York: John Wiley & Sons, 1975.
[12] F. Bastide, “Galileo E5a/E5b and GPS L5 Acquisition Time Statistical Characterization and Application to Civil Aviation,” in *Proc. 2004 Nat. Tech. Meeting Inst. Navigation*, Long Beach, California, Sep. 2004, pp. 1049–1062.
[13] Skybrary, “Approach Speed Categorisation.” 2023. [Online]. Available: https://skybrary.aero/articles/approach-speed-categorisation
[14] B. Parkinson and J. Spiker, *Progress in astronautics and aeronautics: Global positioning system: Theory and applications,* vol. 1. 1996.

Nicolas Gault graduated as an electronic engineer from ENAC (École Nationale de l'Aviation Civile) Toulouse, France, in 2020. He is now a Ph.D student at the TELECOM lab of ENAC. His Ph.D topic deals with the model of impact of interferences on the GNSS L5/E5a band. He recently spent 6 months at the RF & SatNav laboratory of the University of Colorado, Boulder, for collaborative research.

Axel Garcia-Pena is a researcher/lecturer with the SIGnal processing and NAVigation (SIGNAV) research axis of the TELECOM lab of ENAC (French Civil Aviation University), Toulouse, France. His research interests are GNSS navigation message demodulation, optimization and design, GNSS receiver design and GNSS satellite payload. He received his double engineer degree in 2006 in digital communications from SUPAERO and UPC, and his PhD in 2010 from the Department of Mathematics, Computer Science and Telecommunications of the INPT (Polytechnic National Institute of Toulouse), France.

Alexandre Chabory received the M.Sc. degree in electrical engineering from ENAC, the French Civil Aviation University, Toulouse, in 2001, and the Ph.D. degree from Paul Sabatier University, Toulouse, in 2004. From 2004 to 2007, he was a Post-Doctoral Scientist with the Eindhoven University of Technology, the Netherlands. Since 2007, he has been with ENAC where he is now full-professor and heading the electromagnetics and antennas research group. His research interests include electromagnetic theory and modeling, mainly for aeronautical applications.

Christophe Macabiau graduated as an electronic engineer in 1992 from the ENAC (Ecole Nationale de l’Aviation Civile) in Toulouse, France. Since 1994, he has been working on the application of satellite navigation techniques to civil aviation. He received his Ph.D in 1997 and has been in charge of the signal processing lab of ENAC since 2000, where he also started dealing with navigation techniques for terrestrial navigation. He is currently the head of the TELECOM team of ENAC, that includes research groups on signal processing and navigation, electromagnetics, and data communication networks.

Loïc Shi-Garrier is a PhD student at Ecole Nationale de l'Aviation Civile. He received a master's degree in aerospace engineering in 2020 and a master's degree in operational research in 2021, both from ENAC. He is interested in robust machine learning, differential geometry, and air traffic flow and capacity management.